

A methodology to constrain carbon dioxide emissions from coal-fired power plants using satellite observations of co-emitted nitrogen dioxide

Fei Liu^{1,2}, Bryan N. Duncan², Nickolay A. Krotkov², Lok N. Lamsal^{1,2}, Steffen Beirle³, Debora Griffin⁴, Chris A. McLinden⁴, Daniel L. Goldberg⁵, and Zifeng Lu⁵

¹Universities Space Research Association (USRA), Goddard Earth Sciences Technology and Research (GESTAR), Columbia, MD, USA

²NASA Goddard Space Flight Center, Greenbelt, MD, USA

³Max-Planck-Institut für Chemie, Mainz, Germany

⁴Air Quality Research Division, Environment and Climate Change Canada, Toronto, ON, Canada

⁵Energy Systems Division, Argonne National Laboratory, Lemont, IL, USA

Correspondence to: Fei Liu (fei.liu@nasa.gov)

Abstract. We present a method to infer CO₂ emissions from individual power plants based on satellite observations of co-emitted nitrogen dioxide (NO₂), which could serve as complementary verification of bottom-up inventories or be used to supplement these inventories. We demonstrate its utility on eight large and isolated US power plants, where accurate stack emission estimates of both gases are available for comparison. In the first step of our methodology, we infer nitrogen oxides (NO_x) emissions from US power plants using Ozone Monitoring Instrument (OMI) NO₂ tropospheric vertical column densities (VCDs) averaged over the ozone season (May-September) and a “top-down” approach that we previously developed. Second, we determine the relationship between NO_x and CO₂ emissions based on the direct stack emissions measurements reported by continuous emissions monitoring system (CEMS) programs, accounting for coal quality, boiler firing technology, NO_x emission control device type, and any change in operating conditions. Third, we estimate CO₂ emissions for power plants using the OMI-estimated NO_x emissions and the CEMS NO_x/CO₂ emission ratio. We find that the CO₂ emissions estimated by our satellite-based method during 2005–2017 are in reasonable agreement with the US CEMS measurements, with a relative difference of 8% ± 41% (mean ± standard deviation). The broader implication of our methodology is that it has the potential to provide an additional constraint on CO₂ emissions from power plants in regions of the world without reliable emissions accounting. We explore the feasibility by comparing the derived NO_x/CO₂ emission ratios for the US with those from a bottom-up emission inventory for other countries and applying our methodology to a power plant in South Africa, where the satellite-based emission estimates show reasonable consistency with other independent estimates. Though our analysis is limited to a few power plants, we expect to be able to apply our method to more US (and world) power plants when multi-year data records become available from new OMI-like sensors with improved capabilities, such as the Tropospheric Monitoring Instrument (TROPOMI) and upcoming geostationary satellites, such as the Tropospheric Emissions: Monitoring Pollution (TEMPO) instrument.

1 Introduction

Thermal power plants, particularly coal-fired power plants, are among the largest anthropogenic CO₂ emitters, contributing ~40% of energy-related CO₂ emissions globally in 2010 (Janssens-Maenhout et al., 2017). Coal-fired power plants are expected to be one of the primary contributors of CO₂ emissions in the coming decades because of abundant world coal reserves (Shindell and Faluvegi, 2010). Therefore, it is important to accurately monitor global CO₂ emissions from power production in order to better predict climate change (Shindell and Faluvegi, 2010) and to support the development of effective climate mitigation strategies.

1 CO₂ emissions from power plants are typically quantified based on bottom-up approaches using fuel consumption and
2 fuel quality, though fuel properties are not always well known, resulting in uncertainties in the estimated CO₂ emissions for
3 individual plants (Wheeler and Ummel, 2008). Even for US power plants that are considered to have the most accurate
4 information on fuel usage among world nations, the difference between emissions estimated based on fuel usage and those
5 reported as part of continuous emissions monitoring systems (CEMS) programs is typically about 20% (Ackermann and
6 Sundquist, 2008). Thus, emission estimates based on independent data sources, such as satellite observations, are a desirable
7 complement to validate and improve the current CO₂ emissions inventories, especially in countries without CEMS data,
8 which is the case in most of the world.

9 Anthropogenic CO₂ emissions have been estimated from space-based CO₂ observations, but the existing satellite CO₂
10 sensors are designed to provide constraints on natural CO₂ sources and sinks (Basu et al., 2013; Houweling et al, 2015), and
11 thus their capability for monitoring anthropogenic point sources is limited (Nassar et al., 2017). Observations from sensors,
12 including the Scanning Imaging Absorption Spectrometer for Atmospheric Chartography (SCIAMACHY; Burrows et al.,
13 1995), Greenhouse gases Observing SATellite (GOSAT; Yokota et al., 2009), and Orbiting Carbon Observatory-2 (OCO-2;
14 Crisp et al., 2015), show statistically significant enhancements over metropolitan regions (Kort et al., 2012; Schneising et al.,
15 2013; Janardanan et al., 2016; Buchwitz et al., 2018; Reuter et al., 2019; Wang et al., 2018). However, very few studies have
16 focused on individual point sources. Bovensmann et al. (2010) and Velazco et al. (2011) presented a promising satellite
17 remote sensing concept to infer CO₂ emissions for power plants based on the atmospheric CO₂ column distribution. Nassar et
18 al. (2017) presented the first quantification of CO₂ emissions from individual power plants using OCO-2 observations.
19 However, because of the narrow swath (~10 km at nadir) and 16-day repeat cycle of the OCO-2 sensor, the number of clear-
20 day overpasses is too small to allow for the development of a global CO₂ emissions database.

21 In contrast to CO₂, inferring NO_x emissions from individual power plants using satellite NO₂ column retrievals has been
22 done with a higher degree of confidence (e.g., Duncan et al., 2013; de Foy et al., 2015). The Dutch-Finnish Ozone
23 Monitoring Instrument (OMI) on NASA's Earth Observing System Aura spacecraft (Schoeberl et al., 2006) provides near
24 daily, global NO₂ tropospheric VCDs at a spatial resolution of 13×24 km² (at nadir) (Levelt et al., 2006; 2018; Krotkov et al.,
25 2017), which allows emission signals from individual power plants to be resolved. Beirle et al. (2011) first analyzed isolated
26 large sources (i.e., megacities and the US Four Corners power plant) by averaging OMI NO₂ tropospheric VCDs separately
27 for different wind directions, which allows for the estimation of NO_x emissions and lifetimes by fitting an exponentially
28 modified Gaussian function. Several follow-up studies (e.g., de Foy et al., 2015; Lu et al., 2015 and Goldberg et al., 2019a)
29 further developed this approach and inferred NO_x emissions from isolated power plants and cities. More recently, we
30 advanced this approach for sources located in polluted areas to infer NO_x emissions for 17 power plants and 53 cities across
31 China and the US (Liu et al., 2016; 2017).

32 Since NO_x is co-emitted with CO₂, NO_x emissions inferred from satellite data may be used to estimate CO₂ emissions
33 from thermal power plants. Previous analyses estimated regional CO₂ emissions based on satellite-derived NO_x emissions
34 and the NO_x to CO₂ emission ratios from bottom-up emission inventories (Berezin et al., 2013; Kononov et al., 2016;
35 Goldberg et al., 2019b) or co-located satellite retrievals of CO₂ and NO₂ (Reuter et al., 2014). Hakkarainen et al. (2016)
36 confirmed the spatial correlation between CO₂ spatial anomalies and OMI NO₂ VCD enhancements at the regional scale
37 using satellite observations at higher resolution. Hakkarainen et al. (2019) also showed how overlapping OCO-2 CO₂ data
38 and data of NO₂ from the recently launched (October 2017) European Union Copernicus Sentinel 5 precursor
39 TROPospheric Monitoring Instrument (TROPOMI) can be used to identify small scale anthropogenic CO₂ signatures.

40 More recently, the co-located regional enhancements of CO₂ observed by OCO-2 and NO₂ observed by TROPOMI were
41 analysed to infer localized CO₂ emissions for six hotspots including one power plant globally (Reuter et al., 2019). As
42 emissions plumes are significantly longer than the swath width of OCO-2 (10 km), OCO-2 sees only cross sections of

1 plumes, which may not be sufficient to infer emission strengths. Because power plant emissions can have substantial
 2 temporal variations (Velazco et al., 2011) and the cross-sectional CO₂ fluxes are valid only for OCO-2 overpass times, the
 3 cross-sectional fluxes may not adequately represent the annual or monthly averages, which are required for the development
 4 of climate mitigation strategies. In addition, the cross-sectional fluxes may not be a good approximation for emission
 5 strengths if meteorological conditions are not taken into account (Varon et al., 2018). As compared to the method proposed
 6 in this study, Reuter’s method has the advantage of not requiring a priori emission information. However, there are currently
 7 no satellite instruments with a wide enough swath to allow wider application of Reuter’s method.

8 In this study, we present a method to estimate CO₂ emissions from individual power plants using OMI NO₂ observations
 9 and auxiliary CEMS information necessary to estimate NO_x to CO₂ emission ratios. Such estimates could serve as
 10 complementary verification of bottom-up CO₂ inventories or be used to supplement these inventories. For instance, Liu et al.
 11 (2018) used satellite data of SO₂ to identify large SO₂ sources that were missing from a bottom-up emissions inventory and
 12 created a merged bottom-up/top-down SO₂ emissions inventory. We apply our approach to US power plants, which have an
 13 exceptionally detailed CEMS database of NO_x and CO₂ emissions, in order to validate our method. Using auxiliary CEMS
 14 information, we explore the relationship between NO_x and CO₂ emissions for individual power plants, assessing variations in
 15 the ratio associated with coal quality, boiler firing type, NO_x emission control device technology, and changes in operating
 16 conditions. Understanding the causes of these variations will allow for better informed assumptions when applying our
 17 method to power plants that have no or uncertain information on the factors that affect their emissions ratios. We discuss the
 18 uncertainties and applications of our approach, and the potential of NO₂ datasets from new and upcoming satellite
 19 instruments, which will improve the utility of our method for inferring CO₂ emissions from power plants around the world.
 20 Finally, we discuss future research directions.

21 **2 Method**

22 In this section, we present our method to infer CO₂ emissions ($E_{CO_2}^{Sat}$) from satellite-derived NO_x emissions ($E_{NO_x}^{Sat}$) for
 23 individual coal-fired power plants using the following equation:

$$24 \quad E_{CO_2,y}^{Sat} = \frac{E_{NO_x,y}^{Sat}}{ratio_{i,y}^{CEMS}}, \quad (1)$$

25 where i represents coal type and y represents the target year. We demonstrate our method on US power plants since there are
 26 accurate CEMS stack measurements of NO_x and CO₂ emissions with which to validate $E_{CO_2}^{Sat}$. In Section 2.1, we describe
 27 how we estimate $E_{NO_x}^{Sat}$ from OMI NO₂ tropospheric VCD observations. In Section 2.2, we discuss how we estimate the ratio
 28 of NO_x to CO₂ emissions ($ratio_y^{CEMS} = E_{NO_x,y}^{CEMS} / E_{CO_2,y}^{CEMS}$) from CEMS stack measurements in the US Emissions & Generation
 29 Resource Integrated Database (eGRID; USEPA, 2018). Since post-combustion NO_x control systems, including selective
 30 noncatalytic reduction (SNCR) and selective catalytic reduction (SCR), change the relationship between $E_{NO_x}^{CEMS}$ and $E_{CO_2}^{CEMS}$,
 31 we present separate methods to determine $ratio_y^{CEMS}$ for power plants without and with post-combustion NO_x control
 32 systems in Section 2.2.1 and Section 2.2.2, respectively. We discuss the validation of the estimated $E_{CO_2}^{Sat}$ in Section 3.

33 **2.1 Estimating satellite-derived NO_x emissions ($E_{NO_x}^{Sat}$)**

34 From all US coal-fired power plants, we selected 21 power plants for estimating $E_{NO_x}^{Sat}$. We chose these plants based on the
 35 magnitude of their annual emissions (i.e., $E_{NO_x}^{CEMS} > 10$ Gg/yr in 2005) and relative isolation from other large sources to avoid
 36 “contamination” of a power plant’s NO_x plume. Power plants located in urban areas (i.e., within a radius of 100 km from a
 37 city center), or clustered in close proximity (i.e., 50 km) with other large industrial plants were excluded by visual inspection

1 using satellite imagery from Google Earth. We used the top 200 largest US cities (ranked by 2018 population as estimated by
2 the United States Census Bureau, available at https://en.wikipedia.org/wiki/List_of_United_States_cities_by_population) to
3 select power plants. As discussed below, we were able to estimate $E_{NO_x}^{Sat}$ for 8 of the 21 plants. The locations of the 8 plants
4 are shown in Figure 1 and given in Table S1.

5 We followed the method of Liu et al. (2016; 2017) to estimate $E_{NO_x}^{Sat}$ for 2005 to 2017. In our analysis, we used OMI NO₂
6 tropospheric VCDs from the NASA OMI standard product, version 3.1 (Krotkov et al., 2017) together with meteorological
7 wind information from the Modern-Era Retrospective Analysis for Research and Applications, version 2 (MERRA-2; Gelaro
8 et al., 2017). We only analysed data for the ozone season (May-September), in order to exclude winter data, which have
9 larger uncertainties and NO_x lifetimes are longer. As in our previous study (Liu et al., 2017), we calculated 1-dimensional
10 NO₂ “line densities”, i.e. NO₂ per cm, as function of distance for each wind directions separately by integration of the mean
11 NO₂ VCDs (i.e. NO₂ per cm²) perpendicular to the wind direction. We then used the changes of NO₂ line densities under
12 calm wind conditions (wind speed < 2 m/s below 500 m) and windy conditions (wind speed > 2 m/s) to fit the effective NO_x
13 lifetime. We then estimated the average NO₂ total mass integrated around a power plant on the basis of the 3-year mean
14 VCDs, in agreement with previous studies (Fioletov et al., 2011; Lu et al., 2015). The NO₂ total mass was scaled by a factor
15 of 1.32 in order to derive total NO_x mass following Beirle et al. (2011). The uncertainty associated with the NO/NO₂ ratio
16 has been discussed in detail in Section 3 of the supplement in Liu et al. (2016). The 3-year average $E_{NO_x}^{Sat}$ was derived from
17 the corresponding 3-year average NO_x mass divided by the average NO_x lifetime of the entire study period (Liu et al., 2017).
18 Fitting results of insufficient quality (e.g., correlation coefficient of the fitted and observed NO₂ distributions <0.9) were
19 excluded from this analysis, consistent with the criteria in Section 2.2 of Liu et al. (2016). This final filtering left 18 power
20 plants, of which 8 had valid results for all consecutive 3-year periods between 2005 and 2017. More details of the approach
21 are documented in Liu et al. (2017). The fitted lifetimes and other fitting parameters for all power plants are given in Table
22 S1.

23 We use the Rockport power plant (37.9 °N, 87.0 °W) in Indiana to demonstrate our approach. This power plant is
24 particularly well suited for estimating $E_{NO_x}^{Sat}$, because it is a large and isolated NO_x point source. Figure 2 presents the NO₂
25 VCD map around Rockport and the fitted results. Figure 3 displays $E_{NO_x}^{Sat}$ based on 3-year mean VCDs. Each 3-year period is
26 represented by the middle year with an asterisk (e.g., 2006* denotes the period from 2005 to 2007). For comparison to $E_{NO_x}^{Sat}$,
27 $E_{NO_x}^{CEMS}$ is from Air Markets Program Data (available at <https://ampd.epa.gov/ampd/>) and averaged over the period of May to
28 September. For this particular plant, $E_{NO_x}^{Sat}$ is always higher than $E_{NO_x}^{CEMS}$ during the entire period, except the last two years.
29 The coefficient of determination for the entire period is $R^2=0.68$. The relative differences for individual 3-year means
30 (defined as $(E_{NO_x}^{Sat} - E_{NO_x}^{CEMS})/E_{NO_x}^{CEMS}$) range from -20% to 41%, because of the uncertainties of $E_{NO_x}^{Sat}$ as discussed in Section
31 3.2. Both datasets present a declining trend from 2012*. The total declines of 45% and 26% since 2012* in $E_{NO_x}^{Sat}$ and $E_{NO_x}^{CEMS}$
32 are attributed to the 25% decrease in net electricity generation for the plant. The average relative difference of $E_{NO_x}^{Sat}$ and
33 $E_{NO_x}^{CEMS}$ for the 8 plants in this study is $0\% \pm 33\%$, ranging from -58% to 72% for individual 3-year periods (Figure 1).

34 2.2 Estimating NO_x to CO₂ emission ratios using CEMS data (*ratio*^{CEMS})

35 We determined the relationship between $E_{NO_x}^{CEMS}$ and $E_{CO_2}^{CEMS}$ for coal-fired power plants using eGRID information about
36 each plant’s net electric generation, boiler firing technology (e.g., tangential or wall-fired boiler), NO_x control device type,
37 fossil fuel category (i.e., coal, oil, gas and other), and coal quality (i.e., bituminous, lignite, subbituminous, refined and waste
38 coal). We used data of power plants with more than 99% of the fuel burned being coal as reported in eGRID. We analyzed
39 the relationship between $E_{NO_x}^{CEMS}$ and $E_{CO_2}^{CEMS}$ by coal type, as emission characteristics vary widely by coal type.

1 eGRID includes two datasets of emissions for NO_x and CO₂: 1) calculated from fuel consumption data and 2) observed by
 2 stack monitoring (i.e., $E_{NO_x}^{CEMS}$ and $E_{CO_2}^{CEMS}$). Here we focus on eGRID CEMS data as $E_{NO_x}^{CEMS}$ are reported to be highly accurate
 3 with an error of less than 5% (e.g., Glenn et al., 2003). $E_{CO_2}^{CEMS}$ may have larger uncertainties than fuel-based emissions
 4 estimates because of uncertainties in the calculation of flue gas flow (Majanne et al., 2015). Nevertheless, we used $E_{CO_2}^{CEMS}$ to
 5 relate NO_x emissions to CO₂ emissions, since the primary uncertainty of $E_{NO_x}^{CEMS}$ and $E_{CO_2}^{CEMS}$ arises from the calculation of the
 6 flue gas flow, which will cancel in $ratio^{CEMS}$.

7 2.2.1 Coal-fired power plants without post-combustion NO_x control systems

8 We initially limited our analysis to $E_{NO_x}^{CEMS}$ and $E_{CO_2}^{CEMS}$ from coal-fired power plants without post-combustion NO_x control
 9 systems in operation in a given year (Table 1). We find that $E_{NO_x}^{CEMS}$ and $E_{CO_2}^{CEMS}$ have a strong linear relationship (Figure 4). In
 10 Figure 4a, we compare $E_{NO_x}^{CEMS}$ and $E_{CO_2}^{CEMS}$ from power plants (using bituminous coal) by boiler firing type in 2005. We use
 11 bituminous coal-fired plants for illustration, as bituminous coal is the most widely used coal in US power plants. We
 12 analyzed power plants that use cyclone or cell burner boilers separately and exclude them in Figure 4 because they typically
 13 produce higher NO_x emissions than other boiler types (USEPA, 2009; available at
 14 <https://www3.epa.gov/ttn/chief/ap42/ch01/index.html>). A strong linear relationship between $E_{NO_x}^{CEMS}$ and $E_{CO_2}^{CEMS}$ is evident with
 15 excellent correlation ($R^2 = 0.93$, $N = 278$), regardless of boiler firing type. Similar linear relationships exist for other years
 16 (e.g., year 2016 in Figure 4b) and other types of coal (Table 1). The slope of the regression of $E_{NO_x}^{CEMS}$ and $E_{CO_2}^{CEMS}$,
 17 $ratio_{regressed}^{CEMS}$, is assumed by setting the intercept to zero. Table 1 shows $ratio_{regressed,i,y}^{CEMS}$ by coal type and year. In Section
 18 3.1, $ratio_{regressed,i,y}^{CEMS}$ will be applied to approximate $ratio_{i,y}^{CEMS}$ when estimating $E_{CO_2}^{Sat}$ from $E_{NO_x}^{Sat}$ for the 8 plants (Figure 1)
 19 for years before post-combustion control systems were in operation.

20 $ratio_{regressed}^{CEMS}$ for power plants using bituminous coal decreased from 2005 (Figure 4a) to 2016 (Figure 4b) by 31% on
 21 average because of reductions in NO_x emission factors associated with improvements in boiler operations, such as by
 22 optimizing furnace design and operating conditions. The NO_x emissions factors, defined as NO_x emission rates per net
 23 electricity generation (Gg/TW · h), declined by 33% from 2005 to 2016 (Figure 4c). We interpolated $ratio_{regressed}^{CEMS}$ to get
 24 year-specific ratios by coal type for the entire study period, as eGRID data are only available for some years (i.e., 2005,
 25 2007, 2009, 2010, 2012, 2014 and 2016).

26 In addition, $ratio_{regressed}^{CEMS}$ shows significant variation by coal type and year (Figure 5). $ratio_{regressed}^{CEMS}$ is 1.7, 1.3 and 0.91
 27 Gg NO_x/Tg CO₂ for bituminous, subbituminous and lignite coal types in 2005, respectively. A reduction over time in
 28 $ratio_{regressed}^{CEMS}$ is observed for all coal types (Figure 5). $ratio_{regressed}^{CEMS}$ displays a large decrease of 31%, 36% and 20% from
 29 2005 to 2016 for bituminous, subbituminous, and lignite coal types, respectively.

30 2.2.2 Coal-fired power plants with post-combustion NO_x control systems

31 Here, we describe how we estimated $ratio^{CEMS}$ for the entire study period for plants that had post-combustion NO_x
 32 control systems installed at some time during our study period, 2005–2017. The estimation is based on $ratio_{regressed}^{CEMS}$
 33 derived in Section 2.2.1 for plants without post-combustion control systems in operation. We introduce a NO_x removal
 34 efficiency parameter, f , to adjust $ratio_{regressed}^{CEMS}$ for years after the installation of post-combustion control systems,
 35 $ratio^{CEMS-Estimated}$:

$$36 \quad ratio_{i,y}^{CEMS-Estimated} = ratio_{regressed,i,y}^{CEMS} \times (1 - f_y), \quad (2)$$

37 f is commonly measured for individual power plants to describe the performance of their post-combustion NO_x control
 38 systems. It is directly reported by some power plant databases, such as the China coal-fired Power plant Emissions Database

(CPED; Liu et al., 2015). For databases that do not report f , like eGRID used in this study, one can estimate it for an individual power plant by first estimating the unabated emissions per electricity generation, $e_{unabated}$, which is the emission factor before the flue gas enters the post-combustion control system:

$$f_y = \frac{e_{unabated,y} - e_{CEMS,y}}{e_{unabated,y}}, \quad (3)$$

where e_{CEMS} denotes the actual emission factor in terms of CEMS NO_x emissions per net electricity generation (Gg/TW h). $e_{unabated}$ for a given year, $e_{unabated,y}$ is estimated based on the emission per electricity generation for years prior, p , to the installation of the post-combustion control system, $e_{unabated,p}$:

$$e_{unabated,y} = k_y \times e_{unabated,p}, \quad (4)$$

where the scaling factor, k_y , is used to account for the change over time in $e_{unabated}$ associated with improvements in boiler operations discussed in Section 2.2.1. k_y is calculated as the ratio of the averaged $e_{unabated}$ (i.e., the slope of the regression of NO_x emissions on electricity generation) in year, t , to that in year, p .

To assess the reliability of $ratio^{CEMS-Estimated}$, we selected all power plants which had post-combustion devices installed between 2005 and 2016. Figure 6 shows a scatterplot of $ratio^{CEMS}$ (i.e., the ratio of $E_{NO_x}^{CEMS}$ to $E_{CO_2}^{CEMS}$ for individual plants) and $ratio^{CEMS-Estimated}$. We used the NO_x emissions factor in 2005, $e_{unabated,2005}$, to predict the unabated emission factor in 2016, $e_{unabated,2016}$, following Equations (3) and (4) in order to quantify the removal efficiencies for 2016, f_{2016} . $ratio_{2016}^{CEMS-Estimated}$ is based on the estimated f_{2016} and $ratio_{regressed,2016}^{CEMS}$ from Section 2.2.1. $ratio^{CEMS}$ and $ratio^{CEMS-Estimated}$ show good correlation ($R^2 = 0.64$), which increases our confidence that the estimated removal efficiencies approximate the actual efficiencies. The slight underestimation suggested by the slope of 0.85 arises from uncertainties in estimating unabated NO_x emission factors ($e_{unabated,y}$) using Equation (4) and thus removal efficiencies (f), which is a major source of error of $E_{CO_2}^{Sat}$ for power plants that install post-combustion NO_x control systems (see details in Section 3.2).

3 Results and Discussion

In Section 3.1, we present $E_{CO_2}^{Sat}$ for our eight selected power plants and, in Section 3.2, we discuss the uncertainties associated with $E_{CO_2}^{Sat}$. In Section 3.3, we compare the US ratios derived in this study with those from a bottom-up inventory for other regions to explore the potential of applying our method to regions outside the US. We finally apply our approach to one power plant in South Africa, which has several independent estimates for its CO₂ emissions as presented in the scientific literature. Table 2 shows three-year means of $E_{NO_2}^{Sat}$, $E_{NO_2}^{CEMS}$, $E_{CO_2}^{Sat}$ and $E_{CO_2}^{CEMS}$ for eight power plants (Figure 1). Table 3 lists the mean and the standard deviation of the relative differences between $E_{NO_x}^{CEMS}$ and $E_{NO_x}^{Sat}$, and $E_{CO_2}^{CEMS}$ and $E_{CO_2}^{Sat}$ for all eight power plants.

3.1 Satellite-derived CO₂ emissions ($E_{CO_2}^{Sat}$)

Figure 7a is a scatterplot of $E_{CO_2}^{Sat}$ and $E_{CO_2}^{CEMS}$ for the eight power plants (Figure 1), seven of which did not have post-combustion NO_x control systems installed during the study period, 2005–2017. The comparison shows a good correlation, R^2 , of 0.66. The average $E_{CO_2}^{CEMS}$ for all power plants is 2.0 Gg/h and the average $E_{CO_2}^{Sat}$ is 1.8 Gg/h. The relative difference for individual three-year means (defined as $(E_{CO_2}^{Sat} - E_{CO_2}^{CEMS})/E_{CO_2}^{CEMS}$) is 8% ± 41% (mean ± standard deviation). For example, Figure 3 shows $E_{CO_2}^{Sat}$ for the Rockport power plant, which typically has a positive bias as compared to $E_{CO_2}^{CEMS}$ because of a positive bias in $E_{NO_x}^{Sat}$.

1 The time series between $E_{CO_2}^{Sat}$ and $E_{CO_2}^{CEMS}$ are generally consistent, with their annual averages for the eight power plants
 2 exhibiting a declining trend of 5%/yr and 3%/yr from 2006* to 2016* for $E_{CO_2}^{Sat}$ and $E_{CO_2}^{CEMS}$, respectively. The reduction in net
 3 electricity generation is the driving force underlying the emission changes, which decreased by 37% for the eight power
 4 plants from 2005 to 2016, as power producers shut down coal-fired units in favor of cheaper and more flexible natural gas as
 5 well as solar and wind (USEIA, 2018). It is interesting to note that the temporal variations in $E_{CO_2}^{Sat}$ are not as “smooth” as
 6 those in $E_{CO_2}^{CEMS}$, which results from fluctuations in $E_{NO_x}^{Sat}$. Such fluctuations are caused by uncertainties associated with
 7 $E_{NO_x}^{Sat}$ as discussed in Section 3.2. For example, changes in VCDs do not necessarily relate linearly with NO_x emissions (e.g.,
 8 Figure 2 in Duncan et al., 2013) because of temporal variations in meteorology, and nonlinear NO_x chemistry (Valin et al,
 9 2013) and transport. Averaging VCDs for a long-term period (3 years in this study) helps reduce those influences, but small
 10 fluctuations may still exist.

11 3.2 Uncertainties

12 We estimated the uncertainty of $E_{CO_2}^{Sat}$ based on the fit performance of $E_{NO_x}^{Sat}$ and comparison with $E_{CO_2}^{CEMS}$. The major
 13 sources of uncertainty are (a) $E_{NO_x}^{Sat}$ (Liu et al., 2016); (b) $ratio_{regressed}^{CEMS}$; and (c) f . We give the estimated uncertainties of
 14 each source for individual power plants in Table S2.

15 $E_{NO_x}^{Sat}$: The uncertainty of $E_{NO_x}^{Sat}$ is quantified following the method described in Liu et al. (2017), accounting for errors
 16 arising from the fit procedure, the NO_x/NO₂ ratio and OMI NO₂ VCD observations (Liu et al., 2016). The number of 1.32
 17 used for scaling the NO₂ to NO_x ratio is based on assumptions presented in section 6.5.1 of Seinfeld and Pandis (2006) for
 18 “typical urban conditions and noontime sun”. Note that conditions are quite similar in this study because of the overpass time
 19 of OMI close to noon, the selection of cloud-free observations, the focus on the ozone season, and the focus on polluted
 20 regions. A case study of CTM simulations shows an identical value of 1.32 for Paris in summer (Shaiganfar et al., 2017).
 21 The simulated NO_x/NO₂ ratio at the OMI overpass time within the boundary layer (up to 2 km) in a chemistry–climate
 22 model, EMAC (Jöckel et al., 2016), was 1.28 ± 0.08 for polluted ($NO_x > 1 \times 10^{15}$ molec cm⁻²) regions for the July 1, 2005, and
 23 1.32 ± 0.06 on average for the ozone season. However, the coarse grid of EMAC ($2.8^\circ \times 2.8^\circ$ in latitude and longitude) may
 24 not capture the true range of variation of the NO_x/NO₂ ratio. Therefore, we assumed an uncertainty of 20% arising from the
 25 NO_x/NO₂ ratio, double than the standard deviation of the EMAC ratio.

26 Additionally, the tropospheric air mass factors (AMF) used in NO₂ retrievals are based on relatively coarsely-resolved
 27 surface albedo data and a priori NO₂ vertical profile shapes, likely causing low-biased VCDs over strong emission sources
 28 (e.g., Russell et al., 2011; McLinden et al., 2014; Griffin et al., 2019). The average AMF uncertainty of ~30% (see Table 2 in
 29 Boersma et al., 2007) likely contributes to the underestimation of emissions from some power plants in this study. Both
 30 random and systematic (bias) uncertainties in VCDs directly propagates into the uncertainty of $E_{NO_x}^{Sat}$ (see details in the
 31 supplement of Liu et al. (2016) and Section 3.4 of Liu et al. (2017)).

32 The overall uncertainties of $E_{NO_x}^{Sat}$ range from 57% to 64% for all power plants in our analysis, which is comparable with
 33 the level of differences between $E_{NO_x}^{Sat}$ and $E_{NO_x}^{CEMS}$. We expect this uncertainty to be less for new (e.g., TROPOMI) and
 34 upcoming (e.g., NASA Tropospheric Emissions: Monitoring Pollution, TEMPO) OMI-like sensors, which have enhanced
 35 capabilities relative to OMI. Further details are provided in Text S1 of the Supplement.

36 $ratio_{regressed}^{CEMS}$: For power plants without post-combustion devices, $ratio_{regressed}^{CEMS}$ derived from the regression (Figure 4a
 37 & b) and the plant-specific CEMS measurements are within 15%, which is assumed as the uncertainty of the ratio for all
 38 power plants.

39 f : For power plants with post-combustion devices, an additional uncertainty of 20% is applied to reflect the difference
 40 between the predicted and the true removal efficiency as suggested by Figure 6.

1 We assume that their contributions to the overall uncertainty are independent. We then define the total uncertainty,
2 expressed as a 95% confidence interval, as the sum of the root of the quadratic sum of the aforementioned contribution. The
3 overall uncertainties of $E_{CO_2}^{Sat}$ are ~60% for all power plants in our analysis.

4 However, it is worth noting that this uncertainty estimate is rather conservative. The mean and the standard deviation of
5 the relative differences between $E_{NO_x}^{CEMS}$ and $E_{NO_x}^{Sat}$, and $E_{CO_2}^{CEMS}$ and $E_{CO_2}^{Sat}$ for all eight power plants provide a good alternative
6 measure of uncertainties (Table 3). The relative differences are rather small, which are $0\% \pm 33\%$ and $8\% \pm 41\%$ (mean \pm
7 standard deviation) for NO_x and CO_2 , respectively. We additionally calculate the geometric standard deviations (GSDs) of
8 the difference between $E_{CO_2}^{CEMS}$ and $E_{CO_2}^{Sat}$ from 2006* to 2016* for individual power plants in Table S2. The small values of
9 GSDs ranging from 1.07 to 1.31 further improve our confidence in the accuracy of the derived emissions in this study.

10 3.3 Application

11 In this section, we assess the feasibility of applying our method to infer CO_2 emissions ($E_{CO_2}^{Sat}$) for power plants outside the
12 US. We first compare the NO_x to CO_2 emission ratios derived from this study with those from a bottom-up emission
13 database in Section 3.3.1. We then apply the US ratio to a power plant in South Africa in Section 3.3.2.

14 3.3.1 Comparison with bottom-up ratios

15 Figure 8 shows the NO_x to CO_2 emission ratios for 2010 from the global power emissions database (GPED; Tong et al.,
16 2018), which is the only publicly-available bottom-up emission database that reports both NO_x and CO_2 emissions for
17 individual power plants for every country. All countries with over 30 coal-fired power plants in GPED are shown in Figure 8.
18 Not surprisingly, countries with more strict standards in place for NO_x emissions from power plants (i.e., NO_x emission limit
19 value (ELV) $< 200 \text{ mg/m}^3$; hereafter referred to as “more strict countries”) have smaller NO_x to CO_2 ratios (i.e., 1.0 versus
20 2.5 on average) than countries with less strict standard (i.e., NO_x ELV $> 200 \text{ mg/m}^3$; hereafter referred to as “less strict
21 countries”). Additionally, the correlation coefficients are smaller for more strict countries (i.e., 0.82 on average) as compared
22 to less strict countries (i.e., 0.96 on average), because power plants in more strict countries are more likely to have installed
23 post-combustion NO_x control systems, which likely lowered $ratio_y^{CEMS}$, similar to what occurred in the US over our analysis
24 period (Section 2.2.2).

25 We further compare the 2005 US $ratio_{regressed}^{CEMS}$ in Table 1 with the GPED NO_x to CO_2 emission ratios for less strict
26 countries. We chose the 2005 value for comparison based on the following considerations. In 2005, the US EPA issued the
27 Clean Air Interstate Rule (CAIR) to address the interstate transport of ozone and fine particulate matter pollution for eastern
28 US states, which reduced NO_x emissions and, thus, NO_x to CO_2 ratios ($ratio_y^{CEMS}$). However, similar comprehensive control
29 strategies have not been adopted in less strict countries. In this way, the 2005 values are expected to show better consistency
30 with the NO_x to CO_2 ratios of less strict countries than values for more recent years. Note that the GPED database does not
31 give information on ratios by coal type. Therefore, we use $ratio_{regressed}^{CEMS}$ for bituminous coal, which is the most widely used
32 coal type in coal-fired power plants in most countries.

33 The ratios for individual power plants in less strict countries tend to be larger than the US $ratio_{regressed}^{CEMS}$ for 2005,
34 considering that power plants in those countries may not be equipped with any NO_x control devices or even low- NO_x burners,
35 a technology which is widely installed in US power plants with and without post-combustion NO_x control devices. Most
36 ratios range from US 2005 $ratio_{regressed}^{CEMS}$ to 2005 $ratio_{regressed}^{CEMS} + \text{standard deviation}$ (Figure 8). It is no surprise that some
37 less strict countries have ratios higher than this range, which also occurs for some US power plants without post-combustion
38 emission controls (Figure 4). However, there are considerable uncertainties in the GPED database given the scarcity of
39 reliable emissions information in less strict countries. For example, the GPED NO_x and CO_2 emissions estimates for Turkey
40 and Russia, which are outliers in Figure 8, are subject to more assumptions and, thus, larger uncertainties than countries with

1 high-quality country-specific emission data, such as China, which has a high-resolution emissions database (CPED; Liu et al.,
2 2015), and India, which has a database developed by Argonne National Laboratory (Lu et al., 2011).

3 Figure 9 shows a schematic of our methodology to estimate the NO_x to CO₂ emission ratios for power plants outside the
4 US. We adopt different approaches for more and less strict countries. More strict countries, including Canada, European
5 Union (EU) member states, Japan, South Korea, and, more recently, China, usually use CEMS to monitor emissions,
6 particularly from the largest emitters. For power plants with CEMS measurements for both NO_x and CO₂ emissions, it is
7 straightforward to use the measured ratios. However, there is still a significant number of power plants in those countries
8 without CEMS technology, particularly for CO₂ measurements. For example, EU member states do not require power plants
9 to use CEMS for CO₂ reporting and the majority of plants in the EU therefore reports CO₂ emissions based on emission
10 factors (Sloss, 2011). Therefore, we recommend applying our method described in Section 2.2 to infer region-specific ratios
11 for those power plants. The US $ratio_{regressed}^{CEMS}$ could be a less accurate, but reasonable approximation when no CEMS data
12 are available, considering those countries share similar NO_x ELVs for power plants as the US. For less strict countries, we
13 recommend using the 2005 US values by coal type when ratios from countries with similar NO_x emission standard are not
14 available. We also recommend assigning a range from 2005 $ratio_{regressed}^{CEMS}$ to 2005 $ratio_{regressed}^{CEMS}$ + standard deviation,
15 instead of a fixed value, to the ratio for inferring CO₂ emissions, considering the knowledge on ratios from those regions are
16 too few to narrow the constraint.

17 As demonstrated in Section 2.2, our method presented in this study provides a reasonable estimate of the ratio for power
18 plants without post-combustion NO_x control devices with only knowing coal type. Even for regions without reliable
19 emission information, the information on coal type, particularly for large power plants, are very likely publicly-available. For
20 power plants that install post-combustion NO_x control technology, we additionally require the removal efficiency of the
21 device to derive the ratio. The removal efficiency of post-combustion NO_x control devices is usually directly reported, as the
22 operation of such devices is very expensive and is expected to be subject to strict quality control and assurance standards. In
23 contrast to bottom-up approaches, many details are required, including coal type, coal quality, boiler firing type, NO_x
24 emission control device type, and operating condition of boiler and emission control device, when calculating NO_x and CO₂
25 emissions.

26 3.3.2 Application to Matimba power plant in South Africa

27 We apply the methodology shown in Figure 9 to estimate CO₂ emissions from a South African power plant, Matimba,
28 which is a strong isolated NO_x point source (Figure 10). It is a well-studied power plant, having had its emissions estimated
29 using several different methods as reported in the literature. We estimate $E_{NO_x}^{Sat}$ for Matimba from 2005 to 2017 based on
30 OMI NO₂ observations following the approach in Section 2.1. Matimba uses subbituminous coal with a calorific value of ~
31 20 MJ/kg (Makgato and Chirwa, 2017). We apply the ratio ranging from 2005 $ratio_{regressed}^{CEMS}$ to 2005 $ratio_{regressed}^{CEMS}$ +
32 standard deviation to Matimba, following the methodology in Figure 9, considering that South Africa is a less strict country
33 without any post-combustion NO_x control devices (Pretorius et al., 2015). Our derived $E_{CO_2}^{Sat}$ is shown in Figure 11 and
34 fluctuates over time. The growth after 2008* is most likely caused by the increased unit operating hours driven by the desire
35 to meet fully the demand for electricity in South Africa after a period of rolling blackouts (2007–2008) (Duncan et al., 2016).
36 The decline afterwards may be associated with the tripping of generating units at the Matimba because of overload and
37 shortage of coal as reported by South African government news agency (available at [https://www.sanews.gov.za/south-
38 africa/eskom-alone-cannot-solve-our-energy-challenges](https://www.sanews.gov.za/south-africa/eskom-alone-cannot-solve-our-energy-challenges)). The increase in 2016* may be associated with a newly-built power
39 plant, Medupi, which began limited operations in 2015. Note that the range of $E_{CO_2}^{Sat}$ (grey band) in Figure 11 represents the
40 emissions based on a range of NO_x-to-CO₂ ratios, not the uncertainty. We calculate the uncertainty of $E_{CO_2}^{Sat}$ for Matimba
41 following Section 3.2 with an additional uncertainty of ~50% to reflect the fact that the ratio may range from $ratio_{regressed}^{CEMS}$

1 to $ratio_{regressed}^{CEMS} +$ standard deviation. The overall uncertainty of $E_{CO_2}^{Sat}$ for Matimba is 81%, as shown by the error bars in
2 Figure 11.

3 Figure 11 shows $E_{CO_2}^{Sat}$ derived in this study and other independent estimates reported in the literature, including two top-
4 down (Nassar et al., 2017; Reuter et al., 2019) and three bottom-up estimates (Wheeler and Ummel, 2008; Tong et al., 2018;
5 Oda et al., 2018). Despite the uncertainties associated with each of these methods, the CO₂ emissions estimates agree
6 reasonably well, but we do not have sufficient information to understand the differences between these estimates. However,
7 Tong et al. (2018) present in their CPED database both CO₂ and NO_x emissions, which allows us to determine that the
8 difference between $E_{NO_x}^{Sat}$ and the CPED bottom-up estimate contributes significantly to the difference in CO₂ estimates from
9 the two methods. $E_{NO_x}^{Sat}$ for Matimba is 3.8 Mg/h for 2010*, which is 65% smaller than the estimate by Tong et al. (2018) for
10 2010. It is not surprising to see such differences considering the uncertainties of satellite-derived NO_x emissions and bottom-
11 up estimates for power plants without reliable CEMS measurements. For instance, $E_{NO_x}^{Sat}$ is potentially underestimated
12 because of the bias in the OMI NO₂ standard product (version 3.1) associated with a low-resolution static climatology of
13 surface Lambert-Equivalent Reflectivity (OMLER) (Kleipool et al., 2008). We perform a sensitivity analysis by using the
14 preliminary new version of the OMI NO₂ product, which uses new geometry dependent Moderate Resolution Imaging
15 Spectroradiometer (MODIS)-based surface reflectivity. The inferred $E_{NO_x}^{Sat}$ based on the new product is over 10% higher than
16 version 3.1. The bottom-up estimates for Matimba are subject to significant uncertainties as well. For example, Tong et al.
17 (2018) used national total fuel consumption of the power sector for South Africa as reported by the International Energy
18 Agency to estimate fuel consumption at the plant level as detailed fuel consumption for each plant is not currently available.
19 Additionally, they used default NO_x emission factors obtained from the literature because of the absence of country-specific
20 measurement data.

21 **4 Conclusions**

22 In our study, we investigated the feasibility of using satellite data of NO₂ from power plants to infer co-emitted CO₂
23 emissions, which could serve as complementary verification of bottom-up inventories or be used to supplement these
24 inventories that are highly uncertain in many regions of the world. For example, our estimates will serve as an independent
25 check of CO₂ emissions that will be inferred from satellite retrievals of future CO₂ sensors (Bovensmann et al., 2010).
26 Currently, uncertainties in CO₂ emissions from power plants confound national and international efforts to design effective
27 climate mitigation strategies.

28 We estimate NO₂ and CO₂ emissions during the “ozone season” from individual power plants from satellite observations
29 of NO₂ and demonstrate its utility for US power plants, which have accurate CEMS with which to evaluate our method. We
30 systematically identify the sources of variation, such as types of coal, boiler, and NO_x emission control device, and change in
31 operating conditions, which affect the NO_x to CO₂ emissions ratio. Understanding the causes of these variations will allow
32 for better informed assumptions when applying our method to power plants that have no or uncertain information on the
33 factors that affect their emissions ratios. For example, we estimated CO₂ emissions from the large and isolated Matimba
34 power plant in South Africa, finding that our emissions estimate shows reasonable agreement with other independent
35 estimates.

36 We found that it is feasible to infer CO₂ emissions from satellite NO₂ observations, but limitations of the current satellite
37 data (e.g., spatio-temporal resolution, signal-to-noise) only allow us to apply our method to eight large and isolated U.S.
38 power plants. Looking forward, we anticipate that these limitations will diminish for the recently launched (October 2017)
39 TROPOMI, and three upcoming (launches expected in the early 2020s) geostationary instruments (NASA TEMPO;
40 European Space Agency and Copernicus Programme Sentinel-4; Korea Meteorological Administration Geostationary

1 Environment Monitoring Spectrometer, GEMS), which are designed to have superior capabilities to OMI. High resolution
2 TROPOMI observations are capable of describing the spatio-temporal variability of NO₂, even in a relatively small city like
3 Helsinki (Ialongo et al., 2019) and allow estimates of NO_x emissions to be calculated for shorter timeframes (Goldberg et al.,
4 2019c). Higher spatial and temporal resolutions will likely reduce uncertainties in estimates of NO_x emissions as well as
5 allow for the separation of more power plant plumes from nearby sources, thus increasing the number of power plants
6 available for analysis. Therefore, future work will be to apply our method to these new datasets, especially after several years
7 of vetted data become available. Additional future work will include applying our method to other regions of the world with
8 reliable CEMS information, such as Europe, Canada and, more recently, China, to develop a more reliable and complete
9 database with region-specific ratios.

10 **Data availability**

11 The OMI NO₂ and MERRA-2 data can be downloaded from the Goddard Earth Sciences Data and Information Services
12 Center (GES DISC; available at <https://disc.gsfc.nasa.gov/datasets>).

13 **Author contribution**

14 Fei Liu, Bryan N. Duncan, and Nickolay A. Krotkov designed the framework. Fei Liu, Steffen Beirle, Lok N. Lamsal,
15 Debora Griffin, Chris A. McLinden, and Daniel L. Goldberg developed the NO_x emission fitting algorithm and Fei Liu
16 carried it out. Fei Liu and Zifeng Lu analysed the NO_x/CO₂ emission ratio. Fei Liu and Bryan N. Duncan prepared the
17 manuscript with contributions from all co-authors.

19 **Competing interests**

20 The authors declare that they have no conflict of interest.

21 **Acknowledgments**

22 This research has been funded by the NASA's Earth Science Division Atmospheric Composition: Modeling and Analysis
23 Program (ACMAP) and the Aura Science team. The Dutch-Finnish-built OMI instrument is part of the NASA EOS Aura
24 satellite payload. KNMI and the Netherlands Space Agency (NSO) manage the OMI project. We thank the US EPA for
25 making the Emissions & Generation Resource Integrated Database (eGRID) available on line.

26 **References**

- 27 Ackerman, K. V., and Sundquist, E. T.: Comparison of two U.S. power-plant carbon dioxide emissions data sets, *Environ.*
28 *Sci. Technol.*, 42, 5688–5693, doi: 10.1021/es800221q, 2008.
- 29 Basu, S., Guerlet, S., Butz, A., Houweling, S., Hasekamp, O., Aben, I., Krummel, P., Steele, P., Langenfelds, R., Torn, M.,
30 Biraud, S., Stephens, B., Andrews, A., and Worthy, D.: Global CO₂ fluxes estimated from GOSAT retrievals of total column
31 CO₂, *Atmos. Chem. Phys.*, 13, 8695–8717, doi: 10.5194/acp-13-8695-2013, 2013.
- 32 Beirle, S., Boersma, K. F., Platt, U., Lawrence, M. G., and Wagner, T.: Megacity emissions and lifetimes of nitrogen oxides
33 probed from space, *Science*, 333, 1737–1739, 2011.
- 34 Berezin, E. V., Konovalov, I. B., Ciais, P., Richter, A., Tao, S., Janssens-Maenhout, G., Beekmann, M., and Schulze, E. D.:
35 Multiannual changes of CO₂ emissions in China: indirect estimates derived from satellite measurements of tropospheric NO₂
36 columns, *Atmos. Chem. Phys.*, 13, 9415–9438, doi: 10.5194/acp-13-9415-2013, 2013.

1 Boersma, K. F., Eskes, H. J., Dirksen, R. J., van der A, R. J., Veefkind, J. P., Stammes, P., Huijnen, V., Kleipool, Q. L.,
2 Sneep, M., Claas, J., Leitão, J., Richter, A., Zhou, Y., and Brunner, D.: An improved tropospheric NO₂ column retrieval
3 algorithm for the Ozone Monitoring Instrument, *Atmos. Meas. Tech.*, 4, 1905–1928, doi:10.5194/amt-4-1905-2011, 2011.

4 Bovensmann, H., Buchwitz, M., Burrows, J. P., Reuter, M., Krings, T., Gerilowski, K., Schneising, O., Heymann, J.,
5 Tretner, A., and Erzinger, J.: A remote sensing technique for global monitoring of power plant CO₂ emissions from space
6 and related applications, *Atmos. Meas. Tech.*, 3, 781–811, doi: 10.5194/amt-3-781-2010, 2010.

7 Buchwitz, M., Reuter, M., Schneising, O., Nođ, S., Gier, B., Bovensmann, H., Burrows, J. P., Boesch, H., Anand, J., Parker,
8 R. J., Somkuti, P., Detmers, R. G., Hasekamp, O. P., Aben, I., Butz, A., Kuze, A., Suto, H., Yoshida, Y., Crisp, D., and
9 O'Dell, C.: Computation and analysis of atmospheric carbon dioxide annual mean growth rates from satellite observations
10 during 2003–2016, *Atmos. Chem. Phys.*, 18, 17355–17370, doi: 10.5194/acp-18-17355-2018, 2018.

11 Burrows, J. P., Häßle, E., Goede, A. P. H., Visser, H., and Fricke, W.: SCIAMACHY—scanning imaging absorption
12 spectrometer for atmospheric cartography, *Acta Astronaut.*, 35, 445–451, doi: [https://doi.org/10.1016/0094-5765\(94\)00278-](https://doi.org/10.1016/0094-5765(94)00278-)
13 T, 1995.

14 Crisp, D.: Measuring atmospheric carbon dioxide from space with the Orbiting Carbon Observatory-2 (OCO-2), *Proc. SPIE*,
15 9607, 960702, doi: 10.1117/12.2187291, 2015.

16 de Foy, B., Lu, Z., Streets, D. G., Lamsal, L. N., and Duncan, B. N.: Estimates of power plant NO_x emissions and lifetimes
17 from OMI NO₂ satellite retrievals, *Atmos. Environ.*, 116, 1–11, 2015.

18 Duncan, B. N., Yoshida, Y., de Foy, B., Lamsal, L. N., Streets, D. G., Lu, Z., Pickering, K. E., and Krotkov, N. A.: The
19 observed response of Ozone Monitoring Instrument (OMI) NO₂ columns to NO_x emission controls on power plants in the
20 United States: 2005–2011, *Atmos. Environ.*, 81, 102–111, 2013.

21 Fioletov, V. E., McLinden, C. A., Krotkov, N., Moran, M. D., and Yang, K.: Estimation of SO₂ emissions using OMI
22 retrievals, *Geophys. Res. Lett.*, 38, L21811, doi: 10.1029/2011gl049402, 2011.

23 Gelaro, R., McCarty, W., Suárez, M. J., Todling, R., Molod, A., Takacs, L., Randles, C. A., Darmenov, A., Bosilovich, M.
24 G., Reichle, R., Wargan, K., Coy, L., Cullather, R., Draper, C., Akella, S., Buchard, V., Conaty, A., Silva, A. M. d., Gu, W.,
25 Kim, G.-K., Koster, R., Lucchesi, R., Merkova, D., Nielsen, J. E., Partyka, G., Pawson, S., Putman, W., Rienecker, M.,
26 Schubert, S. D., Sienkiewicz, M., and Zhao, B.: The Modern-Era Retrospective Analysis for Research and Applications,
27 Version 2 (MERRA-2), *J. Clim.*, 30, 5419–5454, doi: 10.1175/jcli-d-16-0758.1, 2017.

28 Glenn, C., Logan, T., Vu, B., Walsh, M., and Williams, P.: Evaluation of NO_x Flue Gas Analyzers for Accuracy and Their
29 Applicability for Low-Concentration Measurements AU - Gluck, Steven, J. *Air Waste Manage. Assoc.*, 53, 749–758, doi:
30 10.1080/10473289.2003.10466208, 2003.

31 Goldberg, D. L., Saide, P. E., Lamsal, L. N., de Foy, B., Lu, Z., Woo, J. H., Kim, Y., Kim, J., Gao, M., Carmichael, G., and
32 Streets, D. G.: A top-down assessment using OMI NO₂ suggests an underestimate in the NO_x emissions inventory in Seoul,
33 South Korea, during KORUS-AQ, *Atmos. Chem. Phys.*, 19, 1801–1818, doi: 10.5194/acp-19-1801-2019, 2019a.

34 Goldberg, D. L., Lu, Z., Oda, T., Lamsal, L. N., Liu, F., Griffin, D., McLinden, C. A., Krotkov, N. A., Duncan, B. N., and
35 Streets, D. G.: Exploiting OMI NO₂ satellite observations to infer fossil-fuel CO₂ emissions from U.S. megacities, *Sci. Total*
36 *Environ.*, 695, 133805, doi: <https://doi.org/10.1016/j.scitotenv.2019.133805>, 2019b.

37 Goldberg, D. L., Lu, Z., Streets, D. G., de Foy, B., Griffin, D., McLinden, C. A., Lamsal, L. N., Krotkov, N. A., and Eskes,
38 H.: Enhanced Capabilities of TROPOMI NO₂: Estimating NO_x from North American Cities and Power Plants, *Environ. Sci.*
39 *Technol.*, doi: 10.1021/acs.est.9b04488, 2019c.

40 Griffin, D., Zhao, X., McLinden, C. A., Boersma, F., Bourassa, A., Dammers, E., Degenstein, D., Eskes, H., Fehr, L.,
41 Fioletov, V., Hayden, K., Kharol, S. K., Li, S.-M., Makar, P., Martin, R. V., Mihele, C., Mittermeier, R. L., Krotkov, N.,
42 Sneep, M., Lamsal, L. N., Linden, M. t., Geffen, J. v., Veefkind, P., and Wolde, M.: High-resolution mapping of nitrogen

1 dioxide with TROPOMI: First results and validation over the Canadian oil sands, *Geophys. Res. Lett.*, 46, 1049–1060, doi:
2 10.1029/2018gl081095, 2019.

3 Hakkarainen, J., Ialongo, I., and Tamminen, J.: Direct space-based observations of anthropogenic CO₂ emission areas from
4 OCO-2, *Geophys. Res. Lett.*, 43, 11,400–411,406, doi: 10.1002/2016GL070885, 2016.

5 Hakkarainen, J., Ialongo, I., Maksyutov, S., and Crisp, D.: Analysis of Four Years of Global XCO₂ Anomalies as Seen by
6 Orbiting Carbon Observatory-2, *Remote Sensing*, 11, 850, doi: 10.3390/rs11070850, 2019.

7 Houweling, S., Baker, D., Basu, S., Boesch, H., Butz, A., Chevallier, F., Deng, F., Dlugokencky, E. J., Feng, L., Ganshin,
8 A., Hasekamp, O., Jones, D., Maksyutov, S., Marshall, J., Oda, T., O'Dell, C. W., Oshchepkov, S., Palmer, P. I., Peylin, P.,
9 Poussi, Z., Reum, F., Takagi, H., Yoshida, Y., and Zhuravlev, R.: An intercomparison of inverse models for estimating
10 sources and sinks of CO₂ using GOSAT measurements, *Journal of Geophysical Research: Atmospheres*, 120, 5253–5266,
11 doi:10.1002/2014JD022962, 2015.

12 Ialongo, I., Virta, H., Eskes, H., Hovila, J., and Douros, J.: Comparison of TROPOMI/Sentinel 5 Precursor NO₂
13 observations with ground-based measurements in Helsinki, *Atmos. Meas. Tech. Discuss.*, [https://doi.org/10.5194/amt-2019-](https://doi.org/10.5194/amt-2019-329)
14 329, in review, 2019.

15 Janardanan, R., Maksyutov, S., Oda, T., Saito, M., Kaiser, J. W., Ganshin, A., Stohl, A., Matsunaga, T., Yoshida, Y., and
16 Yokota, T.: Comparing GOSAT observations of localized CO₂ enhancements by large emitters with inventory-based
17 estimates, *Geophys. Res. Lett.*, 43, 3486–3493, doi: 10.1002/2016GL067843, 2016.

18 Janssens-Maenhout, G., Crippa, M., Guizzardi, D., Muntean, M., Schaaf, E., Dentener, F., Bergamaschi, P., Pagliari, V.,
19 Olivier, J. G. J., Peters, J. A. H. W., van Aardenne, J. A., Monni, S., Doering, U., and Petrescu, A. M. R.: EDGAR v4.3.2
20 global atlas of the three major greenhouse gas emissions for the period 1970–2012, *Earth Syst. Sci. Data Discuss.*, 2017, 1–
21 55, doi: 10.5194/essd-2017-79, 2017.

22 Jöckel, P., Tost, H., Pozzer, A., Kunze, M., Kirner, O., Brenninkmeijer, C. A. M., Brinkop, S., Cai, D. S., Dyroff, C.,
23 Eckstein, J., Frank, F., Garny, H., Gottschaldt, K. D., Graf, P., Grewe, V., Kerkweg, A., Kern, B., Matthes, S., Mertens, M.,
24 Meul, S., Neumaier, M., Nützel, M., Oberländer-Hayn, S., Ruhnke, R., Runde, T., Sander, R., Scharffe, D., and Zahn, A.:
25 Earth System Chemistry integrated Modelling (ESCiMo) with the Modular Earth Submodel System (MESSy) version 2.51,
26 *Geosci. Model Dev.*, 9, 1153–1200, doi: 10.5194/gmd-9-1153-2016, 2016.

27 Kleipool, Q. L., Dobber, M. R., de Haan, J. F., and Levelt, P. F.: Earth surface reflectance climatology from 3 years of OMI
28 data, *Journal of Geophysical Research: Atmospheres*, 113, doi: 10.1029/2008jd010290, 2008.

29 Konovalov, I. B., Berezin, E. V., Ciaï, P., Broquet, G., Zhuravlev, R. V., and Janssens-Maenhout, G.: Estimation of fossil-
30 fuel CO₂ emissions using satellite measurements of “proxy” species, *Atmos. Chem. Phys.*, 16, 13509–13540,
31 doi:10.5194/acp-16-13509-2016, 2016.

32 Kort, E. A., Frankenberg, C., Miller, C. E., and Oda, T.: Space-based observations of megacity carbon dioxide, *Geophys.*
33 *Res. Lett.*, 39, L17806, doi: 10.1029/2012GL052738, 2012.

34 Krotkov, N. A., Lamsal, L. N., Celarier, E. A., Swartz, W. H., Marchenko, S. V., Bucsela, E. J., Chan, K. L., Wenig, M., and
35 Zara, M.: The version 3 OMI NO₂ standard product, *Atmos. Meas. Tech.*, 10, 3133–3149, doi: 10.5194/amt-10-3133-2017,
36 2017.

37 Levelt, P. F., van den Oord, G. H. J., Dobber, M. R., Malkki, A., Huib, V., Johan de, V., Stammes, P., Lundell, J. O. V., and
38 Saari, H.: The ozone monitoring instrument, *Geoscience and Remote Sensing, IEEE Transactions on*, 44, 1093–1101, 2006.

39 Levelt, P. F., Joiner, J., Tamminen, J., Veefkind, J. P., Bhartia, P. K., Stein Zweers, D. C., Duncan, B. N., Streets, D. G.,
40 Eskes, H., van der A, R., McLinden, C., Fioletov, V., Carn, S., de Laat, J., DeLand, M., Marchenko, S., McPeters, R.,
41 Ziemke, J., Fu, D., Liu, X., Pickering, K., Apituley, A., González Abad, G., Arola, A., Boersma, F., Chan Miller, C., Chance,
42 K., de Graaf, M., Hakkarainen, J., Hassinen, S., Ialongo, I., Kleipool, Q., Krotkov, N., Li, C., Lamsal, L., Newman, P.,

1 Nowlan, C., Suleiman, R., Tilstra, L. G., Torres, O., Wang, H., and Wargan, K.: The Ozone Monitoring Instrument:
2 overview of 14 years in space, *Atmos. Chem. Phys.*, 18, 5699–5745, doi: 10.5194/acp-18-5699-2018, 2018.

3 Liu, F., Zhang, Q., Tong, D., Zheng, B., Li, M., Huo, H., and He, K. B.: High-resolution inventory of technologies,
4 activities, and emissions of coal-fired power plants in China from 1990 to 2010, *Atmos. Chem. Phys.*, 15, 13299–13317, doi:
5 10.5194/acp-15-13299-2015, 2015.

6 Liu, F., Beirle, S., Zhang, Q., Dörner, S., He, K., and Wagner, T.: NO_x lifetimes and emissions of cities and power plants in
7 polluted background estimated by satellite observations, *Atmos. Chem. Phys.*, 16, 5283–5298, doi: 10.5194/acp-16-5283-
8 2016, 2016.

9 Liu, F., Beirle, S., Zhang, Q., van der A, R. J., Zheng, B., Tong, D., and He, K.: NO_x emission trends over Chinese cities
10 estimated from OMI observations during 2005 to 2015, *Atmos. Chem. Phys.*, 17, 9261–9275, doi: 10.5194/acp-17-9261-
11 2017, 2017.

12 Liu, F., Choi, S., Li, C., Fioletov, V. E., McLinden, C. A., Joiner, J., Krotkov, N. A., Bian, H., Janssens-Maenhout, G.,
13 Darmenov, A. S., and da Silva, A. M.: A new global anthropogenic SO₂ emission inventory for the last decade: a mosaic of
14 satellite-derived and bottom-up emissions, *Atmos. Chem. Phys.*, 18, 16571–16586, doi: 10.5194/acp-18-16571-2018, 2018.

15 Lu, Z., and Streets, D. G.: Increase in NO_x emissions from Indian thermal power plants during 1996–2010: Unit-based
16 inventories and multisatellite observations, *Environ. Sci. Technol.*, 46, 7463–7470, doi: 10.1021/es300831w, 2012.

17 Lu, Z., Streets, D. G., de Foy, B., and Krotkov, N. A.: Ozone Monitoring Instrument observations of interannual increases in
18 SO₂ emissions from Indian coal-fired power plants during 2005–2012, *Environ. Sci. Technol.*, 47, 13993–14000, 2013.

19 Lu, Z., Streets, D. G., de Foy, B., Lamsal, L. N., Duncan, B. N., and Xing, J.: Emissions of nitrogen oxides from US urban
20 areas: estimation from Ozone Monitoring Instrument retrievals for 2005–2014, *Atmos. Chem. Phys.*, 15, 10367–10383, doi:
21 10.5194/acp-15-10367-2015, 2015.

22 Majanne, Y., Korpela, T., Judl, J., Koskela, S., Laukkanen, V., and Häyriinen, A.: Real Time Monitoring of Environmental
23 Efficiency of Power Plants, *IFAC-PapersOnLine*, 48, 495–500, doi: <https://doi.org/10.1016/j.ifacol.2015.12.428>, 2015.

24 Makgato, S., and Chirwa, E.: Characteristics of Thermal Coal used by Power Plants in Waterberg Region of South Africa,
25 *Chemical Engineering Transactions*, 57, 511–516, 10.3303/CET1757086, 2017.

26 McLinden, C. A., Fioletov, V., Boersma, K. F., Kharol, S. K., Krotkov, N., Lamsal, L., Makar, P. A., Martin, R. V.,
27 Veefkind, J. P., and Yang, K.: Improved satellite retrievals of NO₂ and SO₂ over the Canadian oil sands and comparisons
28 with surface measurements, *Atmos. Chem. Phys.*, 14, 3637–3656, doi: 10.5194/acp-14-3637-2014, 2014.

29 Nassar, R., Hill, T. G., McLinden, C. A., Wunch, D., Jones, D. B. A., and Crisp, D.: Quantifying CO₂ Emissions From
30 Individual Power Plants From Space, *Geophys. Res. Lett.*, 44, 10,045–010,053, doi:10.1002/2017GL074702, 2017.

31 Oda, T., Maksyutov, S., and Andres, R. J.: The Open-source Data Inventory for Anthropogenic CO₂, version 2016
32 (ODIAC2016): a global monthly fossil fuel CO₂ gridded emissions data product for tracer transport simulations and surface
33 flux inversions, *Earth Syst. Sci. Data*, 10, 87–107, doi: 10.5194/essd-10-87-2018, 2018.

34 Pretorius, I., Piketh, S., Burger, R., and Neomagus, H.: A perspective on South African coal fired power station emissions,
35 *Journal of Energy in Southern Africa*, 26, 27–40, doi: 10.17159/2413-3051/2015/v26i3a2127, 2015.

36 Reuter, M., Buchwitz, M., Hilboll, A., Richter, A., Schneising, O., Hilker, M., Heymann, J., Bovensmann, H., and Burrows,
37 J. P.: Decreasing emissions of NO_x relative to CO₂ in East Asia inferred from satellite observations, *Nature Geoscience*, 7,
38 792, doi: 10.1038/ngeo2257, 2014.

39 Reuter, M., Buchwitz, M., Schneising, O., Krautwurst, S., O'Dell, C. W., Richter, A., Bovensmann, H., and Burrows, J. P.:
40 Towards monitoring localized CO₂ emissions from space: co-located regional CO₂ and NO₂ enhancements observed by the
41 OCO-2 and S5P satellites, *Atmos. Chem. Phys.*, 19, 9371–9383, doi: 10.5194/acp-19-9371-2019, 2019.

1 Russell, A. R., Perring, A. E., Valin, L. C., Bucsel, E. J., Browne, E. C., Wooldridge, P. J., and Cohen, R. C.: A high spatial
2 resolution retrieval of NO₂ column densities from OMI: method and evaluation, *Atmos. Chem. Phys.*, 11, 8543–8554, doi:
3 10.5194/acp-11-8543-2011, 2011.

4 Schneising, O., Heymann, J., Buchwitz, M., Reuter, M., Bovensmann, H., and Burrows, J. P.: Anthropogenic carbon dioxide
5 source areas observed from space: assessment of regional enhancements and trends, *Atmos. Chem. Phys.*, 13, 2445–2454,
6 doi: 10.5194/acp-13-2445-2013, 2013.

7 Schoeberl, M. R., Douglass, A. R., Hilsenrath, E., Bhartia, P. K., Beer, R., Waters, J. W., Gunson, M. R., Froidevaux, L.,
8 Gille, J. C., and Barnett, J. J.: Overview of the EOS Aura mission, *Geoscience and Remote Sensing, IEEE Transactions on*,
9 44, 1066–1074, 2006.

10 Shaiganfar, R., Beirle, S., Denier van der Gon, H., Jonkers, S., Kuenen, J., Petetin, H., Zhang, Q., Beekmann, M., and
11 Wagner, T.: Estimation of the Paris NO_x emissions from mobile MAX-DOAS observations and CHIMERE model
12 simulations during the MEGAPOLI campaign using the closed integral method, *Atmos. Chem. Phys.*, 17, 7853–7890, doi:
13 10.5194/acp-17-7853-2017, 2017.

14 Shindell, D., and Faluvegi, G.: The net climate impact of coal-fired power plant emissions, *Atmos. Chem. Phys.*, 10, 3247–
15 3260, doi: 10.5194/acp-10-3247-2010, 2010.

16 Sloss, L.: Efficiency and emissions monitoring and reporting, CCC/188, 40, IEA Clean Coal Centre, London, UK, 2011.

17 Tong, D., Zhang, Q., Davis, S. J., Liu, F., Zheng, B., Geng, G., Xue, T., Li, M., Hong, C., Lu, Z., Streets, D. G., Guan, D.,
18 and He, K.: Targeted emission reductions from global super-polluting power plant units, *Nature Sustainability*, 1, 59–68, doi:
19 10.1038/s41893-017-0003-y, 2018.

20 U.S. Energy Information Administration (USEIA), *Electric Power Annual 2017*, available at
21 <https://www.eia.gov/electricity/annual/pdf/epa.pdf> (last access: April 11, 2019), 2018.

22 U.S. Environmental Protection Agency (USEPA), *Compilation of Air Pollutant Emission Factors, AP-42, Fifth Edition*,
23 *Volume 1, Chapter 1*, Washington, D. C., available at: <https://www3.epa.gov/ttn/chieff/ap42/ch01/index.html> (last access:
24 March 20, 2019), 2009.

25 U.S. Environmental Protection Agency (USEPA): *Technical support document for eGRID with year 2016 data (the*
26 *Emissions & Generation Resource Integrated Database)*, Washington, D.C., 2018.

27 Valin, L. C., Russell, A. R., and Cohen, R. C.: Variations of OH radical in an urban plume inferred from NO₂ column
28 measurements, *Geophys. Res. Lett.*, 40, 1856–1860, doi:10.1002/grl.50267, 2013.

29 Varon, D. J., Jacob, D. J., McKeever, J., Jervis, D., Durak, B. O. A., Xia, Y., and Huang, Y.: Quantifying methane point
30 sources from fine-scale satellite observations of atmospheric methane plumes, *Atmos. Meas. Tech.*, 11, 5673–5686, doi:
31 10.5194/amt-11-5673-2018, 2018.

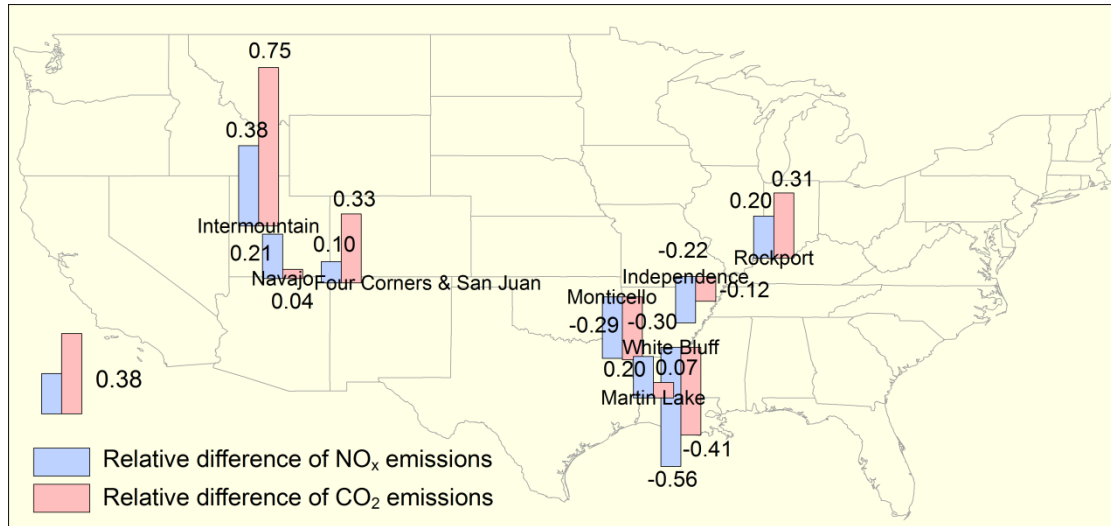
32 Veefkind, J. P., Aben, I., McMullan, K., Förster, H., de Vries, J., Otter, G., Claas, J., Eskes, H. J., de Haan, J. F., Kleipool,
33 Q., van Weele, M., Hasekamp, O., Hoogeveen, R., Landgraf, J., Snel, R., Tol, P., Ingmann, P., Voors, R., Kruizinga, B.,
34 Vink, R., Visser, H., and Levelt, P. F.: TROPOMI on the ESA Sentinel-5 Precursor: A GMES mission for global
35 observations of the atmospheric composition for climate, air quality and ozone layer applications, *Remote Sens. Environ.*,
36 120, 70–83, 2012.

37 Velasco, V. A., Buchwitz, M., Bovensmann, H., Reuter, M., Schneising, O., Heymann, J., Krings, T., Gerilowski, K., and
38 Burrows, J. P.: Towards space based verification of CO₂ emissions from strong localized sources: fossil fuel power plant
39 emissions as seen by a CarbonSat constellation, *Atmos. Meas. Tech.*, 4, 2809–2822, doi: 10.5194/amt-4-2809-2011, 2011.

40 Wang, S., Zhang, Y., Hakkarainen, J., Ju, W., Liu, Y., Jiang, F., and He, W.: Distinguishing anthropogenic CO₂ emissions
41 from different energy intensive industrial sources using OCO-2 observations: A case study in Northern China, *Journal of*
42 *Geophysical Research: Atmospheres*, 123, 9462–9473, doi: 10.1029/2018jd029005, 2018.

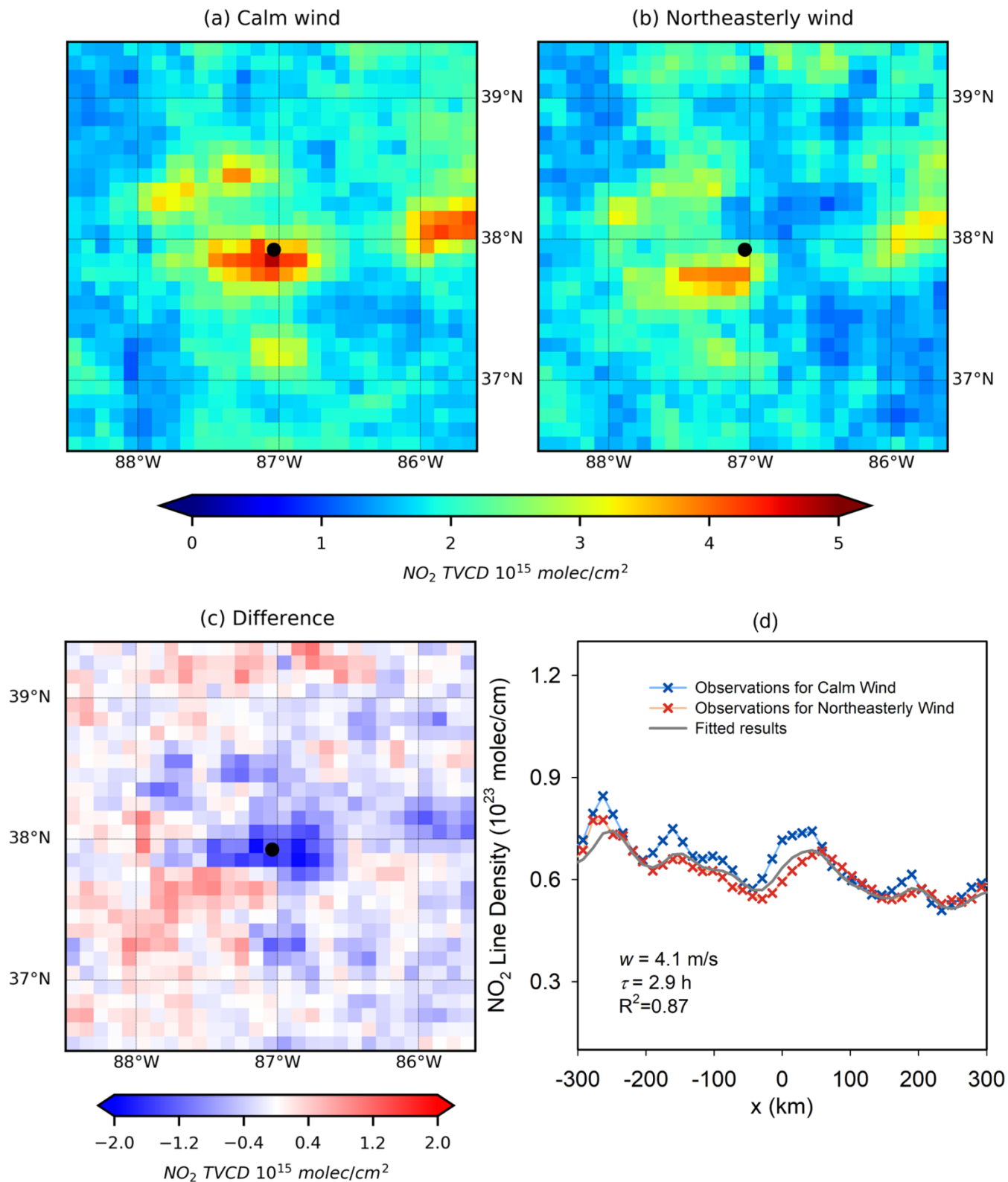
- 1 Wheeler, D., and Ummel, K.: Calculating CARMA: Global estimation of CO₂ emissions from the power sector, Center for
- 2 Global Development, Working Paper 145, 2008.
- 3 Yokota, T., Yoshida, Y., Eguchi, N., Ota, Y., Tanaka, T., Watanabe, H., and Maksyutov, S.: Global Concentrations of CO₂
- 4 and CH₄ Retrieved from GOSAT: First Preliminary Results, SOLA, 5, 160–163, doi: 10.2151/sola.2009-041, 2009.

1 **Figures**

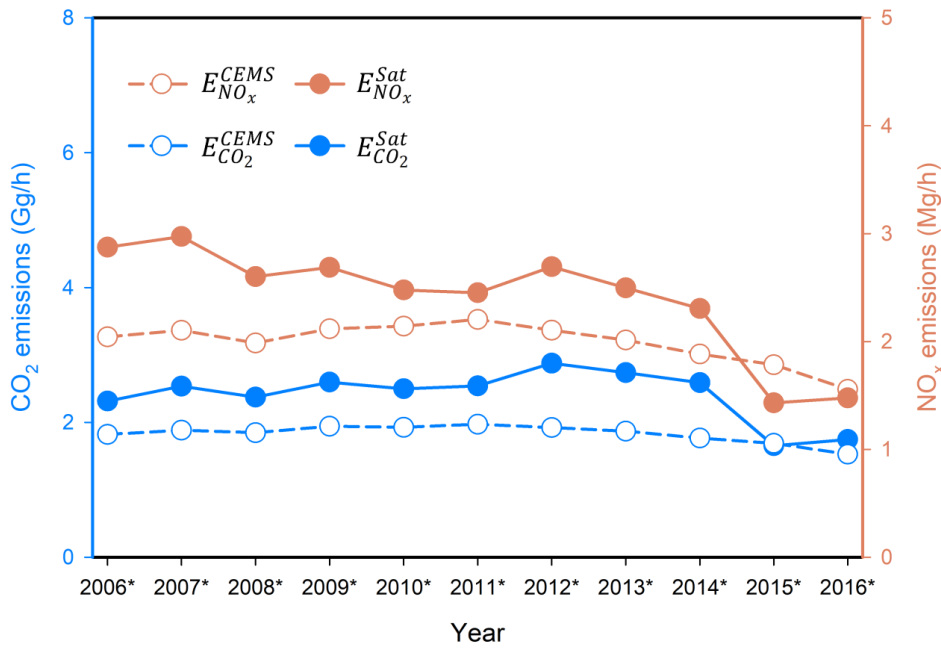


2

3 **Figure 1** Locations of the power plants investigated in this study. The bar charts denote the relative differences, defined as $(E^{Sat} - E^{CEMS})/E^{CEMS}$, averaged over 2005–2017, for NO_x (blue) and CO₂ (red) emissions. The upward and downward bars represent positive and
 4 negative differences, respectively. The Monticello power plant installed SNCR to control NO_x emissions in 2008. The other power plants
 5 are not equipped with post-combustion NO_x control devices.
 6

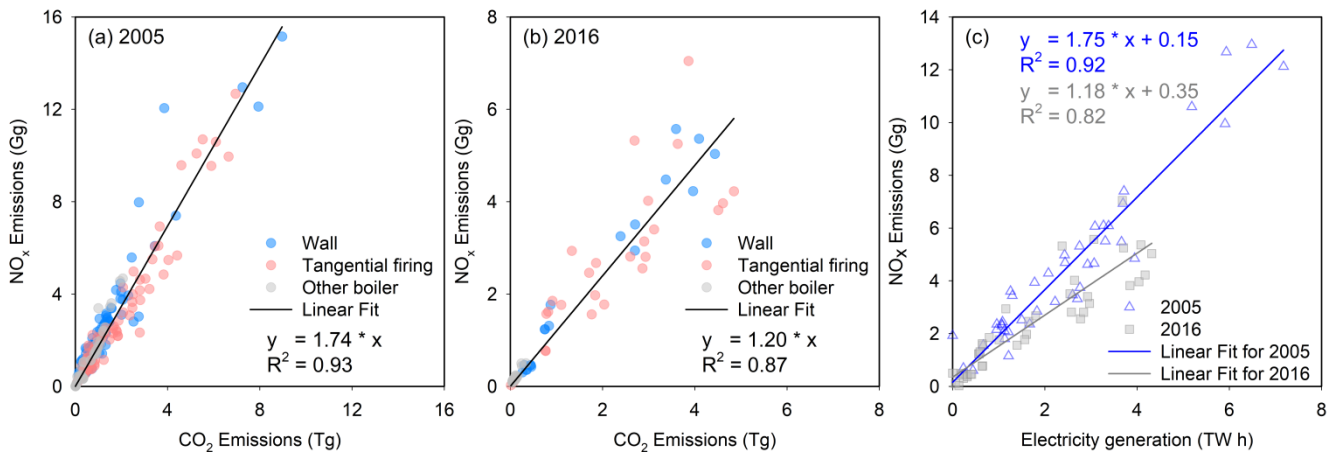


1
 2 **Figure 2** Mean OMI NO₂ tropospheric VCDs around the Rockport power plant (Indiana, USA) for (a) calm conditions, (b) northeasterly
 3 wind and (c) their difference (northeasterly – calm) for the period of 2005 – 2017. The location of Rockport is labelled by a black dot. (d)
 4 NO₂ line densities around Rockport. Crosses: NO₂ line densities for calm (blue) and northeasterly winds (red) as function of the distance *x*
 5 to Rockport center. Grey line: the fitted results for NO₂ line densities for northeasterly winds. The numbers indicate the net mean wind
 6 velocities (windy – calm) from MERRA-2 (*w*), the fitted lifetime (τ), and the coefficient of determination (R^2) of the fit.



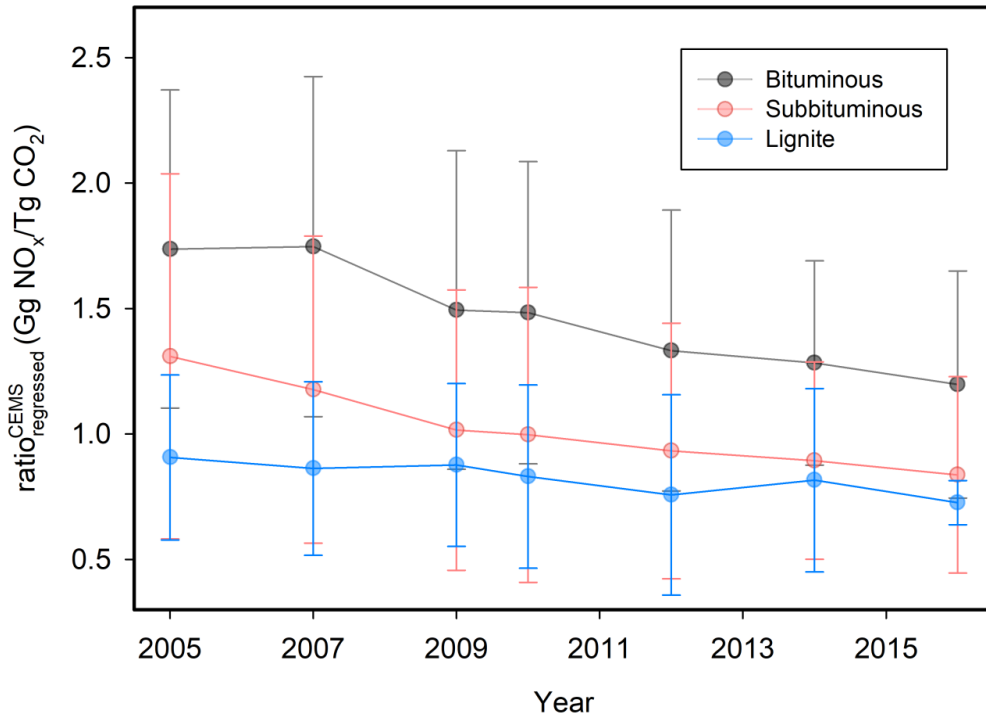
1
2
3
4
5

Figure 3 $E_{NO_x}^{Sat}$ (Mg/h; orange solid lines – right axis) and $E_{CO_2}^{Sat}$ (Gg/h; blue solid line – left axis) for the Rockport power plant from 2005 to 2017. $E_{NO_x}^{CEMS}$ and $E_{CO_2}^{CEMS}$ (dashed lines) are also shown. The 3-year periods are represented by the middle year with an asterisk (e.g., 2006* denotes the period from 2005 to 2007).

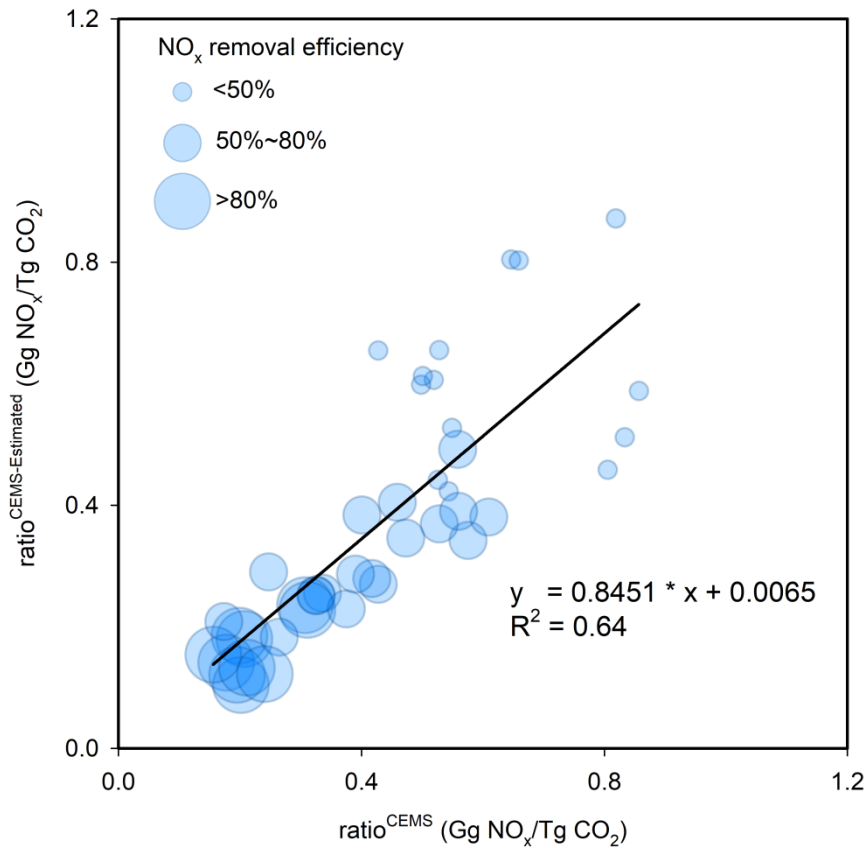


6
7
8
9
10

Figure 4 Scatter plots of $E_{NO_x}^{CEMS}$ versus $E_{CO_2}^{CEMS}$ for all the US bituminous coal-fired electric generating units for (a) 2005 and (b) 2016. Values are color coded by firing type. (c) Scatter plot of $E_{NO_x}^{CEMS}$ versus electricity generation of the same units for years 2005 (triangle) and 2016 (square). Only plants without post-combustion NO_x control devices within a given year are used. The electricity generation data are also from eGRID. The lines in all three panels represent the computed linear regressions.



1
 2 **Figure 5** Interannual trends of $ratio_{regressed}^{CEMS}$ for power plants using bituminous, subbituminous and lignite coal types and without post-
 3 combustion NO_x control devices in a given year. Error bars show the standard deviations for ratios of $E_{NO_x}^{CEMS}$ to $E_{CO_2}^{CEMS}$ for individual power
 4 plants.



5
 6 **Figure 6** Scatterplot of $ratio^{CEMS-Estimated}$ as compared to $ratio^{CEMS}$ for 2016. All 44 coal-fired power plants that operated post-
 7 combustion devices after 2005 and before 2016 (including 2016) are used in the plot. The sizes of the circles denote the magnitude of the
 8 NO_x reduction efficiency of post-combustion control devices estimated in this study. The line represents the linear regression of $ratio^{CEMS}$
 9 to $ratio^{CEMS-Estimated}$.

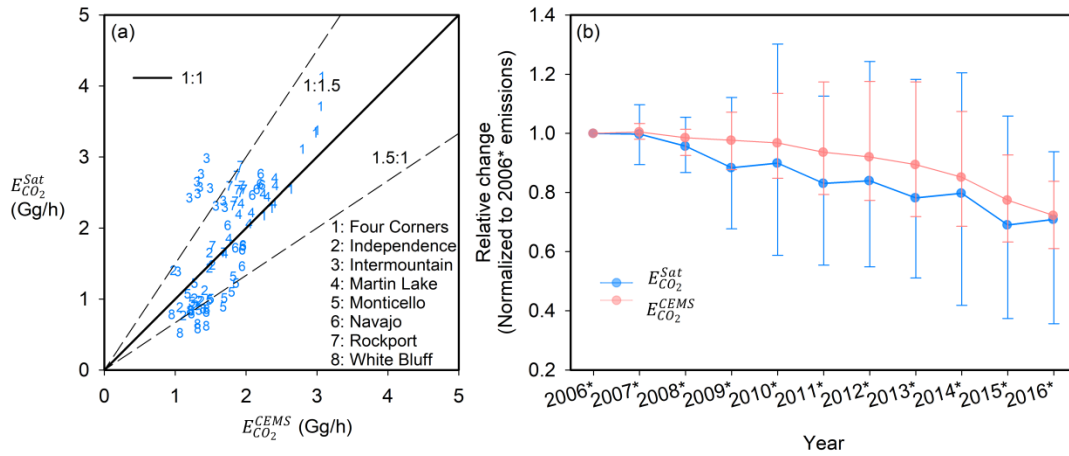


Figure 7 (a) Scatterplot of $E_{CO_2}^{Sat}$ for eight power plants as compared to $E_{CO_2}^{CEMS}$ from 2006* to 2016*. The solid lines represent the ratio of 1:1. The dashed lines represent the ratio of 1:1.5 and 1.5:1, respectively. (b) Interannual trends of the averaged $E_{CO_2}^{Sat}$ (blue lines) and $E_{CO_2}^{CEMS}$ (pink lines) are for all power plants analyzed in this study from 2006*–2016*, as normalized to the 2006* value. The whiskers denote the maximum and minimum values.

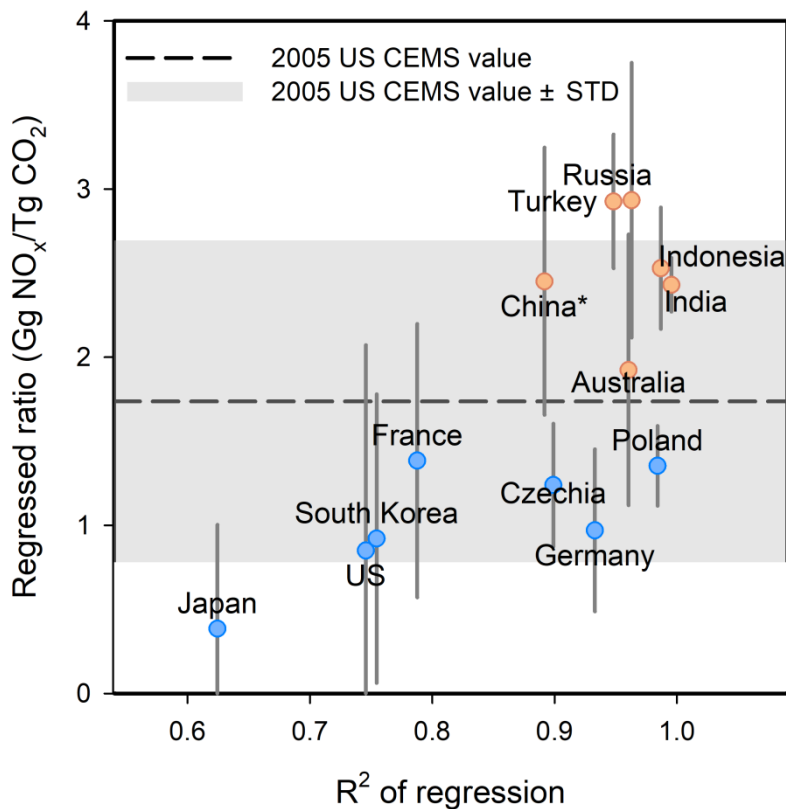


Figure 8 Comparison of the regressed NO_x to CO_2 emission ratios derived from the global power emissions database (GPED) for different regions versus the correlation coefficient of the regression. The blue and red circles denote regions that are subject to more strict standard for NO_x emissions from power plants (i.e., a NO_x ELV of 200 mg/m^3 or less) and other regions, respectively. Y axis: the slope of the regression of the NO_x to CO_2 emissions with an assumed y-intercept of zero. Error bars show the standard deviations for the NO_x to CO_2 emission ratios for individual power plants. X axis: correlation coefficient of the regression. The dashed line represents 2005 US $ratio_{regressed}^{CEMS}$ for bituminous coal derived in this study. The grey shadow represents 2005 US $ratio_{regressed}^{CEMS} \pm$ standard deviation.

*China switched from being a less strict country to a more strict country in 2014, when most coal-fired power plants in China were required to comply with its new emission standards (GB13223-2011).

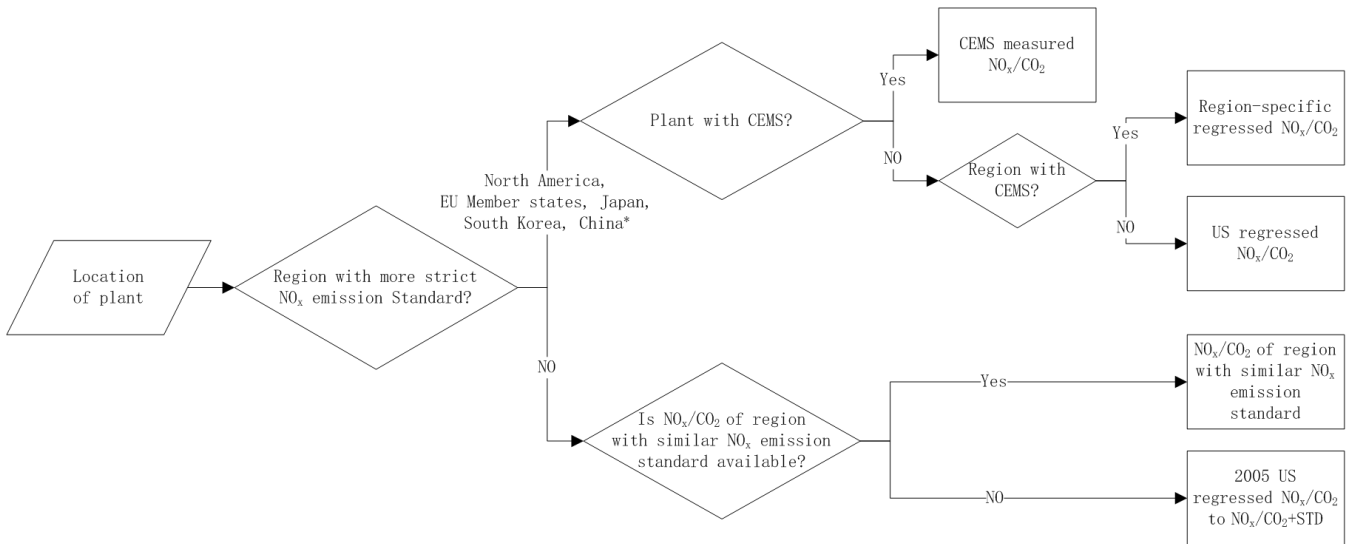


Figure 9 Schematic of our methodology to estimate the NO_x to CO₂ emission ratios for power plants outside the US.

*China switched from being a less strict country to a more strict country in 2014, when most coal-fired power plants in China were required to comply with its new emission standards (GB13223-2011).

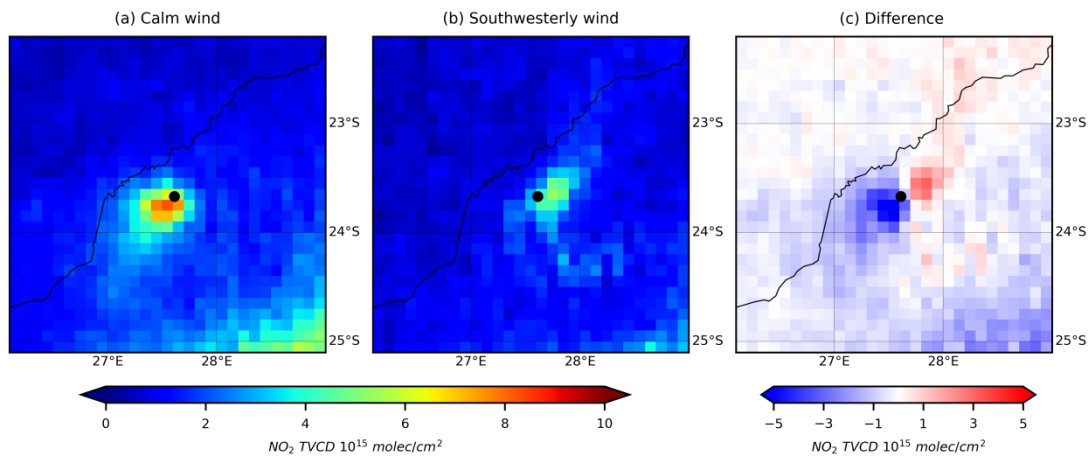


Figure 10 Mean OMI NO₂ tropospheric VCDs around the Matimba power plant (Lephalale, South Africa) for (a) calm, (b) southwesterly wind conditions and (c) their difference (southwesterly – calm) for the period of 2005 – 2017. The location of Matimba is represented by a black dot.

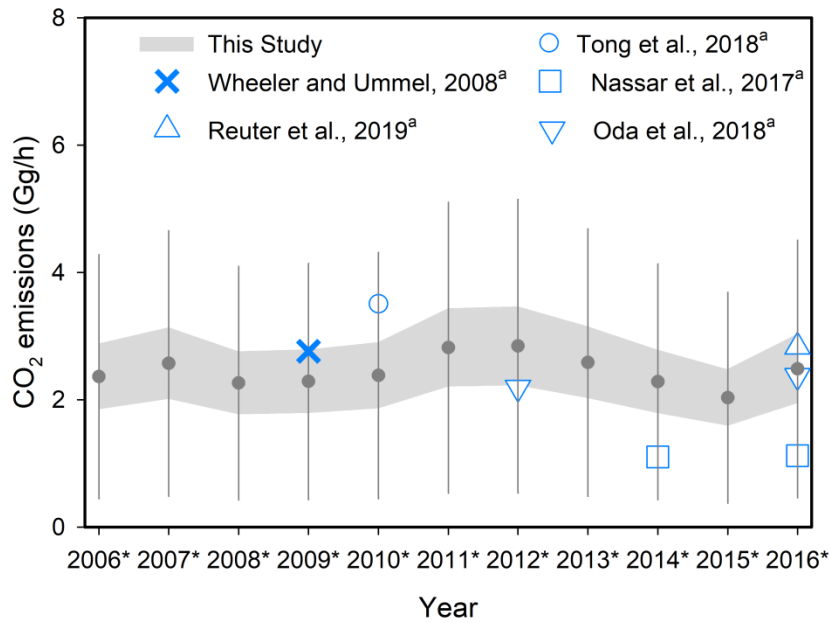


Figure 11 Comparison of $E_{CO_2}^{Sat}$ (Gg/h) derived in this study with existing estimates for the Matimba power plant during 2005 to 2017. $E_{CO_2}^{Sat}$ is inferred based on the NO_x to CO_2 emissions ratio ranging from $ratio_{regressed}^{CEMS}$ to $ratio_{regressed}^{CEMS} +$ standard deviation of ratio. The upper and lower grey bands denote the emissions inferred from $ratio_{regressed}^{CEMS}$ and $ratio_{regressed}^{CEMS} +$ standard deviation of ratio, respectively. The grey dots and error bars show the mean of the upper and lower grey bands and their uncertainties, respectively. ^aEmissions are estimated for 2009 by Wheeler and Ummel (2008); for 2010 by Tong et al. (2018); for 2014 and 2016 by Nassar et al. (2017); for 2016 by Reuter et al. (2019); and for 2012 and 2016 by Oda et al. (2018).

Table 1 The slope ($ratio_{regressed}^{CEMS}$), coefficient of determination, standard deviation and sample number of the linear regression of $E_{NO_x}^{CEMS}$ and $E_{CO_2}^{CEMS}$ by year for all US power plants without post-combustion NO_x control devices from 2005 to 2016.

Coal type	Year	$ratio_{regressed}^{CEMS}$	R ²	Standard deviation	Sample number ^a
Bituminous	2005	1.74	0.93	0.63	278
	2007	1.75	0.91	0.68	286
	2009	1.49	0.88	0.64	241
	2010	1.48	0.86	0.60	235
	2012	1.33	0.87	0.56	190
	2014	1.28	0.87	0.41	136
	2016	1.20	0.87	0.45	66
Subbituminous	2005	1.31	0.65	0.73	226
	2007	1.18	0.61	0.61	221
	2009	1.02	0.66	0.56	230
	2010	1.00	0.67	0.59	216
	2012	0.93	0.74	0.51	200
	2014	0.89	0.74	0.39	165
	2016	0.84	0.70	0.39	111
Lignite	2005	0.91	0.74	0.33	20
	2007	0.86	0.82	0.35	22
	2009	0.88	0.91	0.32	16
	2010	0.83	0.94	0.37	18
	2012	0.76	0.91	0.40	15
	2014	0.82	0.92	0.37	12
	2016	0.73	0.78	0.09	9

^aThe sample number generally decreases from 2005 to 2016 as power plants installed post-combustion NO_x control devices over time.

Table 2 Summary of effective NO_x lifetimes, satellite-derived NO_x emissions ($E_{NO_x}^{Sat}$), CO₂ emissions ($E_{CO_2}^{Sat}$) and bottom-up NO_x emissions ($E_{NO_x}^{CEMS}$), CO₂ emissions ($E_{CO_2}^{CEMS}$) for 8 US power plants during May to September from 2005 to 2017. The 3-year periods are represented by the middle year with an asterisk.

Category	Year	Four Corners & San Juan	Independence	Intermountain	Martin Lake	Monticello	Navajo	Rockport	White Bluff	
NO _x lifetime	2005-2017	2.7	2.5	2.2	2.3	3.2	2.3	2.4	4.3	
$E_{NO_x}^{Sat}$ (Mg/h)	2006*	10.5	2.0	4.0	2.4	1.1	4.6	2.9	1.0	
	2007*	10.0	1.7	4.1	2.3	1.1	4.4	3.0	0.9	
	2008*	9.4	1.6	3.7	2.0	0.8	4.5	2.6	0.9	
	2009*	7.2	1.2	3.9	2.1	0.7	3.9	2.7	0.7	
	2010*	6.8	1.0	4.4	2.1	0.6	3.6	2.5	0.9	
	2011*	6.5	0.9	3.6	1.8	0.7	2.5	2.5	0.8	
	2012*	6.3	0.9	3.4	1.6	0.6	2.3	2.7	0.8	
	2013*	5.6	0.8	3.5	1.8	0.5	1.9	2.5	0.6	
	2014*	4.4	0.7	3.5	1.7	0.8	2.2	2.3	0.5	
	2015*	3.8	0.8	3.0	1.4	0.7	2.1	1.4	0.4	
$E_{NO_x}^{CEMS}$ (Mg/h)	2006*	7.4	1.8	3.0	1.8	1.5	3.8	2.0	1.7	
	2007*	7.3	1.8	3.1	1.8	1.4	3.9	2.1	1.6	
	2008*	6.8	1.8	2.9	1.8	1.3	3.8	2.0	1.6	
	2009*	6.5	1.6	2.9	1.8	1.2	3.4	2.1	1.8	
	2010*	6.2	1.6	2.8	1.7	1.1	2.8	2.1	1.8	
	2011*	6.2	1.4	2.5	1.5	1.0	2.2	2.2	1.9	
	2012*	6.1	1.3	2.4	1.4	0.9	1.9	2.1	1.9	
	2013*	5.6	1.3	2.4	1.3	0.9	1.9	2.0	2.0	
	2014*	5.2	1.2	2.5	1.3	0.8	1.9	1.9	1.9	
	2015*	4.3	1.2	2.0	1.3	0.8	1.7	1.8	1.5	
$(E_{NO_x}^{Sat} - E_{NO_x}^{CEMS}) / E_{NO_x}^{CEMS}$	2005-2017	10%	-22%	38%	20%	-29%	21%	20%	-56%	
	$E_{CO_2}^{Sat}$ (Gg/h)	2006*	6.1	1.6	2.3	2.7	1.2	2.6	2.3	0.8
		2007*	5.9	1.5	2.4	2.6	1.3	2.6	2.5	0.8
		2008*	5.6	1.4	2.3	2.3	1.1	2.8	2.4	0.8
		2009*	4.1	1.1	2.6	2.4	1.0	2.5	2.6	0.6
		2010*	3.7	1.0	3.0	2.5	0.9	2.5	2.5	0.9
		2011*	3.4	1.0	2.6	2.2	1.0	1.7	2.5	0.8
		2012*	3.3	1.0	2.5	2.1	1.0	1.7	2.9	0.9
		2013*	3.1	0.9	2.6	2.3	0.8	1.5	2.7	0.6
		2014*	2.5	0.8	2.8	2.2	1.2	1.8	2.6	0.6
2015*		2.3	0.9	2.4	1.8	1.1	1.7	1.7	0.5	
$E_{CO_2}^{CEMS}$ (Gg/h)	2006*	3.1	1.5	1.7	2.4	1.9	2.2	1.8	1.2	
	2007*	3.1	1.5	1.7	2.4	1.8	2.2	1.9	1.2	
	2008*	3.0	1.5	1.6	2.4	1.8	2.2	1.8	1.2	
	2009*	3.1	1.4	1.5	2.3	1.7	2.1	1.9	1.3	
	2010*	3.0	1.4	1.4	2.2	1.7	2.1	1.9	1.4	
	2011*	3.0	1.3	1.3	2.1	1.5	2.0	2.0	1.4	
	2012*	3.0	1.3	1.3	2.0	1.5	1.9	1.9	1.4	

	2013*	2.8	1.3	1.3	1.9	1.3	1.9	1.9	1.4
	2014*	2.6	1.1	1.4	1.9	1.3	2.0	1.8	1.3
	2015*	2.4	1.1	1.2	1.8	1.2	1.8	1.7	1.1
	2016*	2.2	1.0	1.0	1.7	1.2	1.7	1.5	0.9
<hr/>									
$(E_{CO_2}^{Sat} - E_{CO_2}^{CEMS}) / E_{CO_2}^{CEMS}$	2005-2017	33%	-12%	75%	7%	-30%	4%	31%	-41%

Table 3 Summary of relative difference between satellite-derived NO_x emissions ($E_{NO_x}^{Sat}$) and bottom-up NO_x emissions ($E_{NO_x}^{CEMS}$), satellite-derived CO₂ emissions ($E_{CO_2}^{Sat}$) and bottom-up CO₂ emissions ($E_{CO_2}^{CEMS}$) for 8 US power plants during May to September from 2005 to 2017. The 3-year periods are represented by the middle year with an asterisk.

Year	Relative Difference for NO _x		Relative Difference for CO ₂	
	Mean	Standard Deviation	Mean	Standard Deviation
2006*	15%	29%	17%	39%
2007*	10%	29%	16%	38%
2008*	5%	30%	14%	39%
2009*	-3%	34%	6%	39%
2010*	-1%	38%	9%	46%
2011*	-5%	31%	3%	40%
2012*	-3%	31%	5%	41%
2013*	-4%	38%	4%	49%
2014*	-3%	36%	7%	46%
2015*	-8%	35%	2%	41%
2016*	-2%	29%	8%	22%